UNIVERSIDAD NACIONAL AUTONOMA DE MEXICO

FACULTAD DE QUIMICA

ESTRUCTURA ELECTRONICA DE CUMULOS DE METALES DE TRANSICION.

TESIS
QUE PARA OBTENER EL TITULO DE:
DOCTOR EN QUIMICA (FISICOQUIMICA)
P R E S E N T A
FRANCISCO MIGUEL DE JESUS CASTRO MARTINEZ

MEXICO. D. F., 1991.

ESTRUCTURA ELECTRONICA DE CUMULOS DE METALES DE TRANSICION.

Abstract.

We apply the multiple scattering techniques together with local density exchange correlation potentials to study the electronic structure of transition metal clusters both in free space (molecular boundary conditions) and clusters embebded in the bulk of the material (clusters-in-condensed-matter-boundary-conditions). With this algorithm it is possible to perform a systematic analysis of the local electronic properties for these kind of systems. The results for the Ni_9 and Ni_9-H clusters allows an study of the competitive effects: chemical bond formation vs. magnetization; which determines the electronic properties of a given cluster. The results shows an anisotropic magnetic distribution in Ni_9, whose magnetic moment per atom of 0.45 *spa* is not far away from that of the bulk, 0.49 *spa*, computed with the same technique. Whereas in Ni_9-H the results stress the importance of the *d*-electrons, charge transfer, and changes in the cluster' magnetization during the chemisorption process. By other hand, the picture computed for the nickel and palladium clusters, embebded in the bulk, is not quite different from that given by the more elaborate band theory calculations. For palladium, our results predict a magnetic phase transition when the lattice parameter has increased about 5 *per cent* with respect to the equilibrium value. But our method is not able to determine the nature of the palladium magnetic state, whose electronic structure shows strong similarities with that of ferromagnetic nickel.

Resúmen.

En esta tesis aplicamos las técnicas de dispersión múltiple junto con potenciales locales de intercambio-correlación, para el estudio de la estructura electrónica de cúmulos de metales de transición tanto en espacio libre (condiciones a la frontera de tipo molecular) asi como cúmulos inmersos en el cristal (condiciones a la frontera para cúmulos inmersos en el cristal). Los resultados para los cúmulos de Ni_9 y Ni_9-H permiten un estudio de los efectos competitivos: formación de enlaces químicos *vs.* magnetización, los cuales determinan las propiedades electrónicas de un cúmulo dado. En Ni_9, se encuentra una distribución anisotrópica de la magnetización, cuyo momento por átomo, 0.45 *spa*, no es muy diferente del que ocurre en el cristal, 0.49 *spa*, calculado con el mismo método. Mientras que en Ni_9-H los resultados remarcan la importancia de los electrones tipo *d*, de la transferencia de carga y de los cambios en la magnetización del cúmulo durante el proceso de la quimisorción. Por otra parte, la imagén calculada para los cúmulos de níquel y paladio no es muy diferente de la obtenida con los cálculos de teoría de bandas. En paladio, nuestros resultados predicen una transición de fase magnética cuando el párametro de malla se ha aumentado un 5 *por ciento*, respecto del valor de equilibrio. Pero nuestro método no es capaz de determinar la naturaleza del estado magnético del paladio, cuya estructura electrónica muestra fuertes similaridades con la del níquel ferromagnético.

Introducción.

El objetivo fundamental de esta tesis consiste en calcular, a primeros principios, la estructura electrónica de cúmulos magnéticos de metales de transición en dos situaciones físicas:

i) en espacio libre é ii) inmersos en el seno del cristal,

y estudiar en términos de ella las complejas interacciones metal-metal, metal-impureza, metal-absorbato ó metal-ligante que se generan en un sistema dado que involucre a los metales de transición. La idea central consiste en efectuar un análisis de las siguientes propiedades para los cúmulos : 1) Naturaleza del enlace químico metal-metal, 2) Acoplamientos magnéticos metal-metal. Esto, como punto de partida para tratar de entender la actividad catalítica que exhiben estos cúmulos en espacio libre. Y entonces, estudiar para la Quimisorción: 3) Naturaleza de la unión química metal-absorbato, 4) Cambios en la magnetización del cúmulo inducidos por el absorbato 5) Importancia de la transferencia de carga, metal → absorbato, en la catálisis, étc.

Mientras que para la situación ii) los resultados teóricos de la estructura electrónica harán posible un análisis de la naturaleza del estado magnético local que puede adquirir un cúmulo atrapado en un ambiente dado de espín polarizado. El propósito de este estudio es entender de qué manera actúan las condiciones a la frontera, del tipo *materia condensada*, sobre las funciones de onda monoelectrónicas del cúmulo para promover en él un estado magnético. Esto para el caso particular de los materiales ferromagnéticos usuales: *e.g.* níquel *fcc.* Pero en esta ocasión también discutiremos el cambio de fase *no magnético*

→ *magnético*, que experimenta el paladio *fcc* al aumentar su párametro de malla. Esta última aplicación es importante ya que con un algoritmo calibrado y aplicado, anteriormente, en materiales ferromagnéticos, en la presente investigación se ha logrado describir correctamente tanto al estado paramagnético así como al magnético de un mismo material. Además, en esta misma aplicación el párametro de malla es una variable más del sistema. (En las aplicaciones anteriores del método, las geometrías eran *fijas*: iguales a las estimadas experimentalmente). Nuestro procedimiento también permite predecir el párametro de malla de un cristal dado.

La técnica empleada será el Método Celular de Dispersión Múltiple y se hará uso de funcionales de la densidad para modelar los efectos de intercambio-correlación: CDM-X$\alpha\beta$. Con estos dos ingredientes se puede efectuar un cálculo del tipo *todos los electrones* para sistemas tan complejos como son los cúmulos de metales de transición, en cualquier situación física dada: impurezas magnéticas, transiciones de fase magnéticas, naturaleza de la unión química en los dímeros homo- y heteronucleares, cúmulos, interacción cúmulo-absorbato, étc. A lo largo del desarrollo de este trabajo ilustraremos de qué manera es posible obtener con una sola *herramienta* tanto propiedades típicas del estado sólido (que se calcularían con métodos de teoría de bandas, con una demanda computacional y teórica no deleznables), así como propiedades de cúmulos y moléculas cuyo cálculo se efectuaría, comúnmente, con métodos *ab initio* convencionales de orbitales moleculares (HF + CI, en alguna versión: MCSCF, GVB-vdw, étc.), pero la aplicabilidad de estos métodos, y el de cualquier otro, a sistemas de metales de transición es un reto que pocas veces ha sido éxitosamente resuelto por la química cuántica.

En el método CDM-X$\alpha\beta$ se efectúa una partición del sistema en celdas ó regiones, se elige la forma del potencial en cada una de ellas y los efectos de intercambio-correlación se apróximan mediante funcionales locales de la densidad. De estos ingredientes se derivan las ventajas prácticas del método. Por ejemplo, una de las particiones más comúnes es aquélla en la que las regiones esféricas, asignadas a los sitios atómicos, son tangentes entre si, esta es la partición *muffin-tin*: un potencial esféricamente simétrico dentro de las esferas atómicas combinado con un potencial constante entre dichas esferas (región intersticial). Las soluciones numéricas obtenidas para la parte radial de la ecuación de Schroedinger en las esferas atómicas y un desarrollo en ondas parciales rapidamente convergente para la región intersticial dan lugar a un conjunto de ecuaciones seculares que se puede resolver por técnicas de dispersión múltiple. Esto nos ha permitido estudiar sistemas de gran diversidad y complejidad de los bloques "s"^{1,2}, "p"^{6} y "d"^{7,8} de la tabla periódica.

Por otra parte, en el método celular las interacciones de intercambio-correlación se calculan haciendo uso de la teoria de funcionales de la densidad. El potencial empleado[9], de naturaleza local, es el X$\alpha\beta$. Con dos parámetros (derivables dentro de la teoria misma) este potencial es capaz de tomar en cuenta el intercambio y parte de la correlación electrónica para cualquier elemento de la tabla periódica en cualquier situación física dada. Los valores númericos de los párametros α y β son de 2/3 y de 0.0025, respectivamente, y son los mismos para cualquier elemento de la tabla periódica en cualquier situación física dada. En este sentido α y β son constantes universales. El potencial X$\alpha\beta$

es el que se empleará en la mayoría de los cálculos reportados en esta tésis, este esquema ha sido nuestro *caballo de batalla* en el análisis de la estructura electrónica de una gran variedad de sistemas de los bloques "*s*"[1,2], "*p*"[6], "*d*"[7,8,10] y "*f*"[11] . En nuestro laboratorio hemos encontrado de manera *heuristica* que el valor de 0.0025 para β, reproduce bastante bien tanto a los parámetros moleculares de especies en espacio libre[1,2,7,8] así como a las propiedades electrónicas de cúmulos de metales de transición[10] y de tierras raras[11] en el seno del cristal. En otra palabras, las propiedades de naturaleza local del estado sólido así como algunos efectos que el entorno liquido[6] ejerce sobre una molécula embebida en él también pueden ser analizados con el método X$\alpha\beta$.

Para la calibración y aplicación del método CDM-X$\alpha\beta$ en sistemas del bloque *s* se eligió[1,2] a las moléculas de H_2^+, H_2 y He_2^{2+}, mismas que han sido de notable importancia en el desarrollo de los métodos de Orbitales Moleculares y de Unión Valencia. Nuestros resultados para estas especies son comparables con los cálculos exactos de Bates *et al*[3], de Kolos y Roothaan[4] y con los de Pauling[5]. Los cálculos para el He_2^{2+} y una escueta comparación de estos con los obtenidos mediante Unión Valencia[5] se presentan en el Apéndice B.

Dado el éxito relativo de la etapa anterior, nuestro siguiente intentó consistió en la aplicación del método en sistemas en donde también existiése una contribución orbital de tipo "*p*", además de la de tipo "*s*". En este caso, los compuestos calculados contienen al hidrógeno y a un isótopo de él, el Muon (Mu), y son[6]: el MuBr y el MuHO, así como sus especies correspondientes, el HBr y el H_2O. Todas estas moléculas se calcularon en dos situaciones: 1) en espacio libre y 2) embebidas en el

seno de una solución líquida de bromo. El objetivo de estos cálculos consistió en efectuar un análisis del efecto isotópico en los corrimientos químicos experimentados por el Mu y el H. El resultado de nuestras investigaciones permitió a la *gente* experimental de partículas elementales la asignación de un valor preciso para el momento magnético del Muón. Para mayores detalles veáse el Apéndice A.

Mi incursión en los sistemas de metales de transición se inició propiamente con el cálculo para el dímero homonuclear[7] de MO_2. La naturaleza de la unión química en este dímero, obtenida con el MCDM-X$\alpha\beta$, fué la correcta: en el estado basal de Mo_2 los orbitales moleculares (OM) de carácter *d* son enlazantes y siguen el orden de unión $\sigma > \pi > \delta$, mientras que el OM 5*s*-5*s* exhibe un comportamiento antienlazante. Adicionalmente, los átomos de Mo se encuentran acoplados antiferromagnéticamente en dicho estado. Esta misma imagen fué obtenida mediante cálculos más sofisticados con funcionales locales de la densidad[12] (LSD) y con la técnica de Unión Valencia Generalizada[13]. En sistemas de metales de transición se cuestionaba seriamente[13] el empleo de LSD. Y el cuestionamiento surgió en este terreno porque en funcionales de la densidad el término de intercambio-correlación se aproxima, para cualquier sistema, por el correspondiente para el de un gas homogéneo de electrones . Entonces podría esperarse que LSD no fuése aplicable en el límite de grandes inhomogeneidades de la densidad electrónica como es el caso de átomos o moléculas de elementos de transición, en donde además los electrones se encuentran altamente localizados en los sitios atómicos exhibiéndo diversos ordenamientos magnéticos. Para estos sistemas, los resultados con LSD[12] reproducían mejor a los resultados

experimentales que los obtenidos por GVB[13].

Un sistema de mayor complejidad lo constituye el dímero heteronuclear de NbIr. En esta molécula la naturaleza de la unión química también es múltiple y similar a la de Mo_2: los OM de carácter "d" son enlazantes y los de carácter "s" son antienlazantes en el estado basal. Pero en NbIr los términos iónicos son de igual importancia que los covalentes y se originan de una fuerte tranferencia de carga desde el átomo pobre en electrones d hacia el más rico en ellos. El resultado es la estructura iónica $Nb^{+}Ir^{-}$; en la que los átomos de Nb e Ir se hallan acoplados antiferromagnéticamente en el estado basal: $(Nb^{+})^{4}Ir^{5}$. Por otra parte, a nivel Hartree Fock la transferencia de carga se efectúa en sentido opuesto por el método CDM-Xαβ. Para una discusión más amplia del mecanismo de la transferencia de carga y de otros detalles del cálculo en NbIr véase la recién aparecida refencia 8.

En el Capítulo II se presenta un modelo para estudiar la Chimisorción en metales de transición. Para este propósito se eligió un cúmulo de nueve átomos de níquel dispuestos en la geometría C_{4v}. Este cúmulo, Ni_9, corresponde a la mitad de una celda cúbica centrada en las caras (*fcc*): un átomo central con sus cuatro primeros vecinos más cercanos en el plano (100), más los cuatro vecinos más cercanos del plano inmediato inferior. Las distancias internucleares en este cúmulo corresponden al parámetro de malla, a, del cristal. En este cúmulo las magnetizaciones son: 0.180 espines por átomo (*spa*) para el átomo central cuyo número de coordinación (NC) es de ocho, 0.415 *spa* para los átomos con NC igual a cinco y de 0.563 *spa* para aquéllos con NC igual a tres. O sea que se manifiesta una fuerte competencia entre los efectos

involucrados en la formación de enlaces químicos (apareamiento de electrones ó intercambio interatómico) y los efectos involucrados en la formación de un estado magnético del sistema (interacciones intraatómicas). La magnetización total del cúmulo es de 0.44 *spa* y no es muy distante de la que ocurre en el seno del cristal[10], calculada con esta misma metodología. Pero en espacio libre, además de la distribución anisotrópica de la magnetización en Ni_9, el átomo central se encuentra acoplado antiferromagneticamente con sus ocho primeros vecinos. Los estados magnéticos que puede adquirir un cúmulo, de un metal de transición dado, son aún más complejos ó exóticos que los que ocurren en el cristal mismo. El cúmulo de Ni_9 es capaz de chimisorber a un átomo de hidrógeno, pero con una energía de unión, E_b, muy pequeña, 17 kcal/mol, incluyendo a la energía de punto cero. El valor experimental de esta propiedad es de 63 kcal/mol. La baja capacidad chemisorbente de Ni_9 es una consecuencia de la *buena* unión química que existe entre los átomos de níquel en el cúmulo. Empezando el proceso de autoconsistencia con cada átomo de níquel en la configuración $3d^9 4s^1$ el proceso de formación de enlaces químicos en Ni_9, ha reducido la magnetización desde un valor inicial de 18 espines por cúmulo hasta 4.09 espines por cúmulo. Esta magnetización, de 0.44 *spa* en Ni_9, se reduce a -0.085 *spa* en el estado basal de Ni_9-H: la magnetización del cúmulo muere en la chimisorción. Pero para que este proceso se halla efectuado, el cúmulo de Ni_9 ha movido su nube electrónica, vía los orbitales "d", hacia la región en donde tiene lugar la reacción química. Localmente, el enlace químico cluster-absorbato puede ser visto como el apareamiento usual de electrones: $Ni^{0.60}\uparrow - H^{0.24}\downarrow$.

Finalmente, en el Capítulo I se presentan los resultados para los cúmulos de Pd y Ni, en las estructuras *fcc*, embebidos en el seno del cristal. Nuestros resultados para estos sistemas son comparables con los resultados generados mediante teoría de bandas.

Pero a pesar de su probada utilidad, el método de dispersión múltiple sufre de limitaciones importantes para resolver problemas interesantes de investigación: no se puede tener acceso fácilmente a valores precisos (*exactitud química*) de la energía total. Esto ha impidido: i) la optimización directa de la geometría y el correspondiente análisis vibracional y ii) el cálculo de las energías de disociación y el de otras diferencias de energía que son necesarias para caracterizar a la superficie de energía potencial de un sistema dado. Otras técnicas de cálculo en la aproximación de la combinación lineal de orbitales moleculares, métodos-LCAO, no sufren de estas limitaciones, pero a cambio de esto requieren de fuertes recursos computacionales, ó sea de un servicio de supercómputo, para su implementación y ejecución[14,15]. Estos son los métodos que se estan empleando más ampliamente en el desarrollo actual de la química cuántica de los metales de transición.

REFERENCIAS.

1.- A. Garritz, J. L. Gázquez, M. Castro, and J. Keller, *Int. J. Quantum Chem.* 15, 731 (1979).

2.- M. Castro, J. Keller and O. N. Ventura, *J.* Chem. Phys. 77, 6348, (1982)

3.- D. R. Bates, K. Ledsham, and A.L. Stewart, Phil. Trans. Roy. Soc.(Lond.) A246, 215, (1953).

4.- W. Kolos and C.C.J. Roothaan, Rev. Mod. Phys. 32, 205 (1960).

5.- L. Pauling, *J.* Chem. Phys. 1, 56 (1933).

6.- M. Castro, J. Keller and P. Rius, Hyperfine Interact. 12, 261 (1982).

7.- M. Castro, J. Keller, and P. Mareca, Int. J. Quantum Chem., Quantum Chem. Symp. 15, 429 (1981).

8.- M. Castro, J. Keller, and P.Mareca, Int. J. Quantum Chem. 39, 689 (1991)

9.- F. Herman, J. P. Van Dyke and I. B. Ortenburger, *Phys. Rev. Lett.* 22, 807 (1969).

10.- M. Castro, F. Estrada and V. Soria in *Density Functional Approaches to Chemistry*. Springer-Verlag, Columbus, 1991. Editado por J. K. Labanowsky and J. W. Andzelm. p. 285-291.

11.- J. Keller, M. Castro, and C. Amador, *Physica* 102B, 129 (1980).

12.- B. Delley, A.J. Freeman and D.E. Ellis, Phys. Rev. Lett. 50, 488 (1983).

13.- M. M. Goodgame and W. A. Goddard III, Phys. Rev. Lett. 48, 135 (1982).

14.- *The Challenge of d and f Electrons*, D. R. Salahub and M. C. Zerner, Eds. Symp. Ser. 394, (1989).

15.- *Density Functional Approaches to Chemistry*. Springer-Verlag, Columbus, 1991. Editado por J. K. Labanowsky and J. W. Andzelm.

I.1.–Propiedades Fenomenológicas de Cúmulos de Metales de Transición.

El conocimento de la estructura electrónica de cúmulos metálicos que constan desde unos cuantos átomos hasta cientos de ellos es importante por las siguientes razones fenomenológicas:

i) Los metales de transición manifiestan una gran actividad catalítica cuando se encuentran en la forma de pequeñas particulas dispersas (catálisis heterogenea) de diámetros menores a 100 Å y con cocientes superficie/volúmen muy altos[1,2]; de aquí que las propiedades fisicoquímicas de estos microcristales sean intermedias entre los regimenes atómicos y metálicos (bultos). Un entendimiento de las propiedades electrónicas y estructurales de estas pequeñas particulas metálicas es necesario para la comprensión de cómo es que estos agregados actúan como catalizadores.

Mediante la condensación súbita de vapores producidos por un láser, se han logrado sintetizar cúmulos aislados de MT de cualquier tamaño[3,4,5]. Esto ha hecho posible el estudio sistemático de algunas propiedades de los cúmulos metálicos. Así se ha encontrado que el comportamiento de la actividad catalítica, en función del tamaño de la particula, exhibe una estructura complicada en los cúmulos del fierro (Fe_n)[3,4], mientras que para los de cobalto y niquel (Co_n y Ni_n) la capacidad catalítica converge monotónicamente, en función de n, a la de la superficie correspondiente[5]. En el caso del fierro, la actividad catalítica de cúmulos muy pequeños, como el de Fe_{10}, se encuentra altamente exhacerbada, respecto de la de sus vecinos (y no difiere mucho de la del bulto) mientras que en otros cúmulos, como en el Fe_{15}, la

capacidad catalítica se encuentra anormalmente suprimida. Finalmente, a partir de Fe_{23} la actividad catalítica de los cúmulos, $Fe_{n\geq 23}$, converge suavemente a la del bulto ó superficie. Adicionalmente, también se ha logrado determinar el número de moléculas chimisorbidas con los que se satura cada uno de estos cúmulos. La explicación de todos estos detalles no se puede dar solo en términos de parametros estructurales ó geómetricos: necesariamente debe darse en términos de la estructura electrónica para explicar racionalmente tendencias y/o anomalías.

ii) Mediante técnicas espectrométricas de masas a altas temperaturas se han obtenido las energías de unión (D_o) de un gran número de moléculas diátomicas homonucleares. Actualmente, se tienen resultados para todos los dímeros de la primera serie de los elementos de transición[6]. Para la segunda serie quedan por determinar las D_o para Zr_2, Tc_2 y Ru_2; mientras que para la tercera serie las D_o aún son muy escasas. Sin embargo, el conjunto de datos experimentales es ya lo sufientemente completo para establecer tendencias y/o anomalías de la energía de unión en estas especies[7]. El reto para la comunidad de químicos teóricos consiste en contestar cuál es la naturaleza de la unión química en estos dímeros en los que las entidades atómicas exhiben configuraciones de valencia del tipo $(n+1)s^1nd^{x+1}$. Se anticipan uniones y enlaces múltiples diferentes a los tradicionales que ocurren entre átomos con configuraciones tipo "sp". Los dímeros son importantes porque representan los sistemas más simples en donde es posible analizar teóricamente la interacción metal-metal. Las energías de cohesión de los metales y, por otra parte, las energías de unión, D_o, de los dímeros siguen tendencias similares a

lo largo de la primera serie de transición[7,8]: algunas interacciones metal-metal se encuentran ya de manera incipiente en el dímero[7,8].

iii) Con las técnicas de aislamiento matricial a bajas temperaturas se pueden formar cúmulos de diferentes tamaño mediante la agregación controlada de átomos del metal[2,8,9]. En consecuencia, es posible seguir los cambios que sufre el espectro de absorción U.V. y visible en función del tamaño del cúmulo[10]. Esto es importante porque entonces podremos "seguir" la génesis de la estructura electrónica de los metales de transición. En esta situación la estructura electrónica de los cúmulos se puede usar para entender como es que los electrones localizados en una molécula se transforman en estados deslocalizados en el metal. Este cambio "enlace" → "banda" es de interés tanto para físicos como para químicos. Frecuentemente se pregunta a qué nuclearidad las propiedades atómicas y moleculares admiten un comportamiento genuinamente metálico.

iv) El magnetismo de estos pequeños cúmulos también es un problema fascinante. Mientras que en la fase condensada algunos metales no exhiben ordenamientos magnéticos, pequeños cúmulos de sus átomos u otros sistemas de menor dimensionalidad , tales como superficies ó interfaces, pueden adquirir propiedades magnéticas[11,12] . En algunos casos las superficies exhiben una magnetización mayor a la del seno del cristal[13].

Para explicar toda esta diversidad de comportamientos que exhiben los metales de transición es necesario desarrollar tratamientos teóricos, en el marco de la mecánica cuántica, para al menos balbucear alguna respuesta.

I.2.-Estado Actual del Arte de los Cálculos Teóricos en Cúmulos de MT.

El cálculo de las propiedades electrónicas de cúmulos de metales de transición representa *per se* un reto para el desarrollo de nuevos métodos de cálculo, é implementación de los ya existentes, para lograr su correcta aplicabilidad a dichos sistemas[14]. Esto es debido a las siguientes razones.

Los metales de transición se caracterizan por presentar configuraciones de valencia del tipo $(n+1)s^1nd^{x+1}$, $(n+1)s^2nd^x$, d^x ó alguna mezcla de estos arreglos. Pero en cualquier caso se tendría una capa *d* relativamente compacta y con un gran número de electrones (hasta un máximo de 10) y una capa *s* altamente deslocalizada y pobremente ocupada. Los problemas en el desarrollo de la química cuántica de los metales de transición se originan, justamente, al intentar describir a este conjunto de electrones *sd* cuya distribución espacial y de espín es altamente intrincada.

La dificultad mayor derivada de las configuraciones *sd* es la *correlación electrónica*. En principio este problema se puede resolver por el método de interacción de configuraciones, CI, en alguna de sus variantes. En estos esquemas la función de onda exacta del sistema se desarrolla como una combinación lineal de determinantes de Slater

$$\Psi_i(1,2,\ldots,N) = \sum_P C_{Pi}\ \Phi_P(1,2,..,N) \quad . \qquad (1)$$

Una vez que los coeficientes del desarrollo han sido determinados, vía el principio variacional, la energía total así como otros observables

del sistema se pueden calcular siguiendo el procedimiento usual, como los valores esperados de los operadores apropiados:

$$< \hat{O} > = < \Psi_1 \mid \hat{O} \mid \Psi_1 > \quad . \qquad (2)$$

Pero esto es bien conocido desde hace algunas décadas y, de antemano, la realización práctica de un cálculo CI, de gran exactitud, es inmediata. En este contexto CI se usa en un sentído general é incluye a todas sus variantes: MCSCF - Método Múlticonfiguracional de Campo Autoconsistente, GVB - Unión Valencia Generalizada, MBPT - Teoria de Perturbaciones de Muchos Cuerpos, étc. Entonces, el éxito ó fracaso de un cálculo CI no reside en el establecimiento de sus bases sólidas formales sino más bien en cuestiones técnicas de procedimiento: concretamente recae sobre la elección del mejor conjunto de funciones determinantales, $\{\Phi_p\}$, para expresar el desarrollo de Ψ. Los recursos computacionales restringen fuertemente esta elección ya que usualmente se requiere un número inmenso de determinantes de Slater para generar un *buen* desarrollo de Ψ. Sin embargo, gracias a la experiencia é ingenio *artesanal* de la comunidad de químicos cuánticos *ab initio* se pueden realizar actualmente cálculos CI para moléculas que contengan hasta una docena de átomos de la segunda (Li-Ne) ó tercera (Na-Ar) serie. En estos cálculos los conjuntos base han sido bien determinados y la elección de las configuraciones más importantes (aquéllas de mayor contribución a la energía de correlación), se lleva a cabo de acuerdo a criterios razonables y controlados. La aplicación de la *tecnología* CI a moléculas

pequeñas ó ligeras se realiza casi de manera automática y, sin demandar grandes esfuerzos computacionales, se puede obtener exactitud química para una propiedad dada del sistema con este tipo de métodos.

Sin embargo, el progreso de la tecnología CI en sistemas de metales de transición es aún incipiente ya que no se cuenta ni con la experiencia requerida para la formulación de reglas y procedimientos ni con métodos CI lo suficientemente desarrollados para determinar *a priori* el esfuerzo requerido para el cálculo de una propiedad dada del sistema, en un estado dado, con una exactitud dada: la solución Hartree-Fock resulta ser una pobre aproximación y el subsecuente desarrollo multideterminantal converge muy lentamente. A pesar de esto, existe una intensa actividad en el terreno de los CI para lograr este objetivo. Con estos métodos se han obtenido resultados de gran exactitud química[15] para la interacción de un *solo* átomo de transición (*e. g.* Cu, Pd ó Pt) y un ligante dado (*e. g.* H_2, N_2, CH_4, C_2H_2), estos resultados teóricos comparan directamente con los resultados experimentales obtenidos mediante las técnicas de aislamiento matricial[15]. Pero este algoritmo CI no ha sido aplicado al análisis de la interacción de un cúmulo de metales de transición (dos ó más átomos de MT) y un ligante dado, M_n-L, al mismo nivel de exactitud que el obtenido para el caso M-L. Es evidente que los resultados teóricos para el caso M_n-L estarían más cerca del proceso catalítico que ocurre en la superficie de un metal de transición dado. En vista de esto se deben buscar métodos alternativos a los CI, para que la química cuántica pueda lograr sus propias contribuciones en la interpretación y/o explicación de los resultados experimentales recientes que se están obteniendo en las diferentes áreas

de la química de los metales de transición. Una de las alternativas a las técnicas CI, son los métodos que se basan en la teoría de funcionales de la densidad (DFT)[16]. Estos métodos han logrado demostrar su aplicación a sistemas de metales de transición de mayor complejidad que los tratados por CI[16,17]. El método de cálculo empleado en esta tesis cae dentro del área de DFT. Volveremos sobre esto más adelante.

Pero además de la correlación electrónica también existen otros retos, de naturaleza no-trivial, en la química cuántica de los metales de transición: i) Cuando se tienen capas abiertas tipo *d* se genera un número inmenso de estados moléculares con una gran diversidad de multiplicidades. ii) En esta misma situación los acoplamientos magnéticos que aparecen en los dímeros ó cúmulos son muy complicados de tratar si se tiene en cuenta que, adicionalmente, el enlace metal-metal que ocurre en estos sistemas usualmente es múltiple, hasta un máximo de seis!. iii) En los metales de transición, algunos electrones del carozo *invaden* la parte espacial de los electrones de valencia, de aquí que también surgan problemas al definir el espacio de Hilbert para los electrones de valencias y del carozo. iv) Además, este último tipo de electrones se mueve a velocidades muy grandes, lo que requeriría de correcciones relativistas para una buena descripción de los sistemas, sobre todo en los de la segunda y tercera serie de transición.

Este es el reto para la química cuántica de los metales de transición. Los métodos de cálculo que actualmente se estan desarrollando para resolver este problema, son extraordinariamente poderosos y sofisticados[14,15,16,17], y en consecuencia requieren de fuertes recursos humanos y computacionales.

I.3.- El Método de la Teoría de Funcionales Locales de la Densidad.

Los métodos de cálculo de la mecánica cuántica que se basan en la teoría de los funcionales de la densidad (DFT)[18,19] son alternativas útiles y prácticas, en adición a los métodos *ab initio* tradicionales, para la descripción *a primeros principios* de las interacciones electrónicas en sistemas que contienen un número, N, de electrones relativamente grande. Las raíces del desarrollo de DFT se encuentran justamente en el tratamiento pre-cuántico del *gas de electrones* realizado por Drude en 1900 al diseñar, por vez primera, un modelo del estado metálico[20,21], después del descubrimiento del electrón. Una versión propiamente cuántica de este *gas electrónico* fué llevada a cabo por Sommerfeld al describir apropiadamente al sistema con la estadística de Fermi-Dirac[21]. Estas ideas fueron incorporadas, posteriormente, en el esquema del átomo conocido como el modelo de Thomas-Fermi-Dirac[22]. Finalmente en la década de los 1960 Hohenberg y Kohn[18] y Kohn y Sham[19] cimentaron las bases formales de la teoría. Una primera extensión de la teoría, para el caso de *spin no restringido* fué formulada en 1972[23]. Un poco después, el primer método que incorpora los resultados de la teoría de una manera práctica para el cálculo de la estructura electrónica de átomos y moléculas aparece en 1975[24]. A continuación expondremos brevemente los aspectos más significativos contenidos en DFT.

Consideremos a un sistema de N-electrones que se mueve en el potencial externo producido por los M núcleos de una molécula ó de un cristal, entonces, siguiendo a Hohenberg y Khon[18] el Hamiltoniano del sistema se puede escribir de la siguiente manera:

$$\hat{H} = \hat{T} + \hat{V} + \hat{U} \quad , \qquad (3)$$

en donde

$$\hat{T} = \sum_{i=1}^{N} -\frac{1}{2}\nabla_i^2 \quad , \qquad (4)$$

$$\hat{V} = \sum v(r_i) = \sum_{i=1}^{N}\sum_{k=1}^{M} \frac{Z_k}{r_i - R_k} \quad , \qquad (5)$$

y

$$\hat{U} = \sum_{i>j}^{N} \frac{1}{r_{ij}} \quad . \qquad (6)$$

Con la definición del funcional universal

$$F[\rho(r)] \equiv \langle \Psi \mid \hat{T} + \hat{U} \mid \Psi \rangle \quad , \qquad (7)$$

del funcional de la energia

$$E_v[\rho(r)] = \int v(r)\,\rho(r)dr + F[\rho(r)] \quad , \qquad (8)$$

y haciendo uso del principio variacional, esto es, que E_v sea mínima para la densidad verdadera del estado basal, Hohenberg y Khon

demostraron que la función de onda total del sistema, Ψ (1,2,...,N), es un funcional único de la densidad electrónica

$$\rho(r) = N \int | \Psi |^2 \, dr_2 \ldots dr_N ds_1 \ldots ds_N \quad . \qquad (9)$$

Aunque el funcional $F[\rho(r)]$ existe y está formalmente definido por la ecuación 7, (en términos de la función de onda total del sistema, la cual a su vez esta determinada por la densidad electrónica, $\rho(r)$) no se conoce la dependencia funcional explícita de F, ni la de E, en términos de ρ. Lo que da lugar a ciertas aproximaciones.

Khon y Sham diseñaron un esquema práctico de ecuaciones de trabajo. Primero que nada *cocinaron* aparte la interacción Culómbica *clásica* contenida en $F[\rho(r)]$:

$$F[\rho(r)] = \frac{1}{2} \int \frac{\rho(r)\rho(r')}{| r - r' |} \, dr \, dr' + G[\rho(r)] \qquad (10)$$

en donde el nuevo funcional universal $G[\rho(r)]$, contiene a la energía cinética y a las interaciones de intercambio-correlación. Y para un mejor manejo de $F[\rho(r)]$, $G[\rho(r)]$ es separado en dos términos:

$$G[\rho(r)] \equiv T_s[\rho(r)] + E_{xc}[\rho(r)] \qquad (11)$$

en donde T_s representa a la energía cinética de un sistema de electrones *no-interactuantes* de densidad $\rho(\mathbf{r})$ mientras que $E_{xc}[\rho(\mathbf{r})]$ contiene a las energías de intercambio y correlación de un sistema *interactuante* de electrones. ($E_{xc}[\rho(\mathbf{r})]$ contiene a la energía *usual* de intercambio-correlación más la diferencia en energía cinética entre un sistema de partículas interactuante y uno no-interactuante, de densidad $\rho(\mathbf{r})$). Ahora, si se efectúan variaciones al funcional de la energía, pero sujetas a la condición de normalización:

$$\int \delta\rho(\mathbf{r})d\mathbf{r} = 0 \qquad (12)$$

se tiene que resultan las siguientes ecuaciones de Euler:

$$\frac{\delta T_s[\rho(\mathbf{r})]}{\delta\rho(\mathbf{r})} + v(\mathbf{r}) + \int \frac{\rho(\mathbf{r}')d\mathbf{r}'}{|\mathbf{r} - \mathbf{r}'|} + \frac{\delta E_{xc}[\rho(\mathbf{r})]}{\delta\rho(\mathbf{r})} = 0 \quad . \quad (13)$$

La ecuación anterior es exacta; sin embargo contiene a un funcional desconocido, $E_{xc}[\rho(\mathbf{r})]$. Si se aplicase el procedimiento anterior a un sistema de partículas *no-interactuantes* que se mueven en un potencial "externo" definido por los tres últimos términos de la ecuación (13), entonces resultarían las mismas ecuaciones de Euler, ya que por definición en un sistema no-interactuante no hay intercambio-correlación y además T_s se definió justamente como la energía cinética de un sistema no-interactuante de partículas. Pero para un sistema de partículas no-interactuantes la ecuación de Schroedinger es separable, de tal manera que la ecuación (13) también se puede expresar de la siguiente

forma (como un conjunto de ecuaciones tipo Hartree):

$$-\frac{1}{2}\nabla^2 + v(r) + \int \frac{\rho(r')dr'}{|r - r'|} + \frac{\delta E_{xc}[\rho(r)]}{\delta\rho(r)} = 0 \quad . \qquad (14)$$

en donde

$$v(\rho(r))_{xc} = \frac{\delta E_{xc}[\rho(r)]}{\delta\rho(r)} \qquad (15)$$

y

$$\rho(r) = \sum_{i=1}^{N} |\Psi_i(r)|^2 \quad . \qquad (16)$$

Aún asi, las ecuaciones de Kohn-Sham, (14)-(16), son exactas. Pero para su aplicación práctica, como siempre ocurre, es necesario efectuar ciertas aproximaciones. (Pero, qué es fundamentalmente la teoria de los funcionales de la densidad?. En pocas palabras DFT es una versión de la teoria cuántica ó mecánica ondulatoria en la que el ente central es justamente la densidad electrónica del sistema. En DFT dada la $\rho(r)$, estimada experimental ó teóricamente, se puede conocer en principio toda la información posible del sistema. En la versión de Schroedinger de la mecánica cuántica la función de onda del sistema, Ψ, desempeña el mismo papel que ρ en DFT. Sin embargo, dado que ρ es un ente menos abstracto que Ψ, probablemente DFT adquiera una mayor aceptación por parte de los investigadores experimentales y de los estudiantes de física ó química.) Ahora si, vienen las aproximaciones.

Si $\rho(r)$ no experimenta grandes variaciones, sino que varía *suavemente*, entonces se origina la *celebre* aproximación local de la densidad (LDA) para el funcional $E[\rho(r)]$:

$$E[\rho(r)] = \int \rho(r)\varepsilon_{xc}(\rho(r))dr \quad , \qquad (17)$$

en donde $\varepsilon_{xc}(\rho(r))$ es la energía de intercambio y correlación por particula (ε_{xc} incluye al término de la energía cinética residual) de un gas homogéneo de electrones *interactuantes* de densidad $\rho(r)$. Entonces el potencial de intercambio-correlación en la aproximación LDA, para las ecuaciones de Kohn-Sham, se define como:

$$v(\rho(r))_{xc} = \frac{d[\rho(r)\varepsilon_{xc}(\rho(r))]}{d\rho(r)} \quad . \qquad (18)$$

El esquema LDA ó su generalización para el caso de espín-polarizado, la aproximación local de la densidad de espín (LSD), proveen de un método que permite involucrar a los efectos de intercambio-correlación, sobre la base del comportamiento local de un gas homogéneo de electrones: el resultado es un conjunto de ecuaciones autoconsistentes, de tipo Hartree, las cuales contienen únicamente operadores locales en el potencial (*efectivo*).

La forma especifica de las ecuaciones LSD dependende del tratamiento efectuado al término de intercambio-correlación. Si

solamente se considera a la interacción de intercambio, entonces se tiene[19,25]

$$v_x^{\uparrow}(\rho(r)) = -\frac{2}{3}\left(\frac{81}{4\pi}\right)^{1/3}\rho(r)^{1/3} \qquad (19)$$

con una expresión similar para $v_x^{\downarrow}(\rho(r))$. Este potencial de intercambio difiere por un factor de 2/3 del derivado por Slater[24,26] y por un factor de $2/3\alpha$ del frecuentemente citado potencial X_α[24]. El intercambio de Slater fué derivado a partir de las ecuaciones monoelectrónicas de Hartree-Fock, promediando en ellas el agujero de Fermi y haciendo uso de la aproximación LSD. El procedimiento de Gaspar fué inverso al de Slater. Gaspar efectúo las aproximaciones (promedio del término de intercambio y LSD) en la expresión de la energía total Hartree-Fock, aplicando después el principio variacional, esto da el potencial de la ecuación 19. Desafortunadamente, este trabajo fué ignorado durante algunos años. El redescubrimiento de la Ec. 19 por Khon y Sham en 1965 dió lugar a ciertas comparaciones entre el potencial de Slater y el de Gaspar-Khon-Sham. Fué así como se originó pués la introducción del párametro de escalamiento, α, ó sea el método X_α.

Pero el artículo de Khon y Sham fué mucho más que el mero redescubrimiento de un método Hartree-Fock apróximado: fundó las bases de la teoría de los funcionales de la densidad y abrió y pavimentó el camino para el tratamiento apróximado, pero sistemático, de los efectos de intercambio-correlación a través del uso de la aproximación LSD en conjunción con cálculos en gases de electrones correlacionados[23,27-29].

La aproximación LSD es a la teoría de los funcionales de la densidad lo que la aproximación Hartree-Fock es a la teoría de la función de onda (métodos *ab initio* convencionales): proveen de un nivel de aproximación útil para efectuar el cálculo en una gran variedad de sistemas y propiedades. Pero LSD tiene ciertas ventajas sobre Hartree-Fock ya que requiere de menos recursos computacionales y además, parte de la correlación electrónica está incluida en el modelo del gas de electrones: en LDA, se incluyen en un solo cálculo tanto efectos de intercambio como de correlación. Esta es la virtud, ahora el defecto. La principal desventaja en local-DFT, consiste en la ausencia de un procedimiento práctico y riguroso para corregir los errores inherentes que arrastra ó conlleva la aproximación local. En los últimos años se han estado desarrollado funcionales cada vez más exactos, pero la mayoría de estos trabajos formales aun no son lo suficientemente prácticos como para implementarlos en los esquemas computacionales.

Las técnicas existentes que van más allá de la aproximación local, al tratar de corregirla, se pueden clasificar en tres categorías. Los métodos que corrigen la auto-interaccion (SIC) se concentran en corregir un error de la aproximación LSD: la cancelación inexacta de los términos auto-culómbicos por los de auto-intercambio-correlación Pero estrictamente hablando éstos no son propiamente métodos de funcionales de la densidad ya que las correcciones involucradas se efectúan sobre orbitales individuales. La segunda categoría emplea intercambio Hartree-Fock exacto y una aproximación local para la energía de correlacion (ó local + SIC). Finalmente, la tercera categoría involucra un desarrollo de gradientes de los términos de intercambio-correlación

para tomar en cuenta las inhomogeneidades de la densidad electrónica en un sistema real. A continuación expondremos algunos detalles principales de cada una de estas técnicas.

I.- Correcciones de auto-intercambio. En la teoria de Hartree-Fock, que no es más que la teoria de la función de onda más sencilla que involucra correctamente la antisimetria del sistema, la repulsión electrónica de un sistema de N-electrones esta dada por

$$< V_{ee}^{HF} > = \sum_{i<j} (J_{ij} - K_{ij}) \qquad (20)$$

en donde las integrales culómbicas, J_{ij}, y de intercambio, K_{ij}, estan definidas sobre los espín-orbitales como

$$J_{ij} = \int\int \psi_i^*(1)\psi_j^*(2)\frac{1}{|r_1 - r_2|}\psi_i(1)\psi_j(2) \qquad (21)$$

$$K_{ij} = \int\int \psi_i^*(1)\psi_j^*(2)\frac{1}{|r_1 - r_2|}\psi_j(1)\psi_i(2) \qquad (22)$$

Ya que $K_{ii} = J_{ii}$, la ecuación (20) se podría escribir como una suma irrestricta, de la siguiente manera:

$$\langle V_{ee}^{HF} \rangle = \frac{1}{2} \sum_{i,j}^{N} (J_{ij} - K_{ij}) \qquad (23)$$

En esta suma las integrales de autointercambio, K_{ii}, sirven únicamente para cancelar a las integrales auto-culómbicas, J_{ii}.

Y ya que la densidad electrónica esta dada por

$$\rho(r_1) = \sum_{i}^{N} \psi_i^*(r_1)\psi_i(r_1) \quad , \qquad (24)$$

$\langle V_{ee}^{HF} \rangle$ se puede escribir de la siguiente forma

$$\langle V_{ee}^{HF} \rangle = \frac{1}{2} \int\int \rho(r_1) \frac{1}{|r_1 - r_2|} \rho(r_2) dr_1 dr_2 \quad - \quad \frac{1}{2} \sum_{i,j} K_{ij} \quad . \quad (25)$$

En teoría de funcionales de la densidad se suele definir a la energía culómbica (directa) por el primer término del lado derecho de la ecuación (25). El funcional de la energía de intercambio-correlación exacto, $E_{xc}[\rho(r)]$, cancela totalmente a las repulsiones auto-culómbicas espurias y, además, toma en cuenta a los efectos de intercambio y de correlación verdaderos. Pero en los funcionales aproximados de LSD no ocurre esto. Por ejemplo, para el átomo de hidrógeno la auto-interaación es de 8.5 *eV* y el 93% de esta energía espuria es cancelada dentro de la aproximación local LSD[30,31].

Perdew y Zunger han enumerado un número de inexactitudes de la

aproximación LSD que son atribuibles a efectos espurios de los términos de la auto-interacción[30] . Pero ellos mismos proponen un esquema para corregirlos. La corrección se lleva a cabo orbital por orbital. Para mayor abundancia se remite al lector a la referencia original.

II.- Intercambio Hartree-Fock más Correlación Local (ó SIC). Otra de las apróximaciones más comunes consiste en emplear a los funcionales de la densidad únicamente para el cálculo de la energía de correlación y evaluar el intercambio con la expresión de Hartree-Fock: la idea de esta estrategia es que las integrales auto-Culómbicas sean propiamente canceladas por las de auto-intercambio; pero para bien ó para mal, esto remitiría otra vez a un nivel HF como punto de referencia. Adicionalmente las demandas computacionales serían del mismo orden de magnitud que las requeridas en los cálculos HF mismos. Algunos resultados de este formalismo han sido resumidos por Stoll *et al*[32]. Si la aproximación local de la densidad se usa para el cálculo de la energía de correlación:

$$E_c[\rho] = \int \rho\ \varepsilon_c(\rho)\ d\mathbf{r} \qquad , \qquad (17)$$

en donde ε_c es la densidad de energía de correlación y ρ es la densidad de un gas homogéneo de electrones, entonces se tiene que: a) la energía de correlación es sobreestimada por un factor de 2, b) se obtienen *buenas* diferencias de energías de correlación entre sistemas de capas cerradas y c) se obtienen resultados no del todo satisfactorios para las diferencias de las energías de correlación entre un sistema de capa cerrada y uno de capa abierta. La fuente principal del error se atribuye

a una energia de autocorrelación residual[33]. En principio esto se podría remediar substrayendo las contribuciones a la E_c provenientes de los electrones del mismo espín. Calculadas éstas con LSD. Al efectuar esto, se obtiene una mejora del 10% en los errores de E_c para átomos[34] si se emplea el potencial de Gunnarson-Lundqvist, el cual no es precisamente uno de los esquemas más exactos elaborados con funcionales locales de la densidad.

Por otro lado Vosko y Wilk[35] han investigado a los funcionales de la energia de correlacion diseñados para corregir la autointeracción de tal manera que se cumplas dos cosas i) E_c es cero para sistemas de un solo electrón y ii) E_c se reduce a LSD en el limite de densidades electrónicas que varian suavemente. Su expresión preferida es:

$$E_c^A[\rho^\uparrow,\rho^\downarrow] = E_c^{LSD}[\rho^\uparrow,\rho^\downarrow] - \sum_\sigma N_\sigma E_c^{LSD}[\rho_\sigma/N_\sigma,0]$$

$$= \sum_\sigma \int \rho_\sigma [\varepsilon_c[\rho^\uparrow,\rho^\downarrow] - \varepsilon_c[\rho_\sigma/N_\sigma,0]$$

en donde N_σ es el número total de electrones de espín σ. Esto es equivalente a remover la autocorrelación de N_σ distribuciones electrónicas cada una de densidad ρ_σ/N_σ, de manera similar a la correción Fermi-Amaldi[36] efectuada a la teoría de Thomas-Fermi. Esta procedimiento fué aplicado a un número de átomos y Vosko y Wilk concluyeron que el intercambio HF más la aproximación de la correlación

local es superior al esquema LSD para el cálculo de energías totales y de densidades para un espín dado, $\rho(\mathbf{r})$, pero que los efectos no-locales son aún sustanciales en el cálculo de $\rho(\mathbf{r})$, aunque se incluyan términos tipo SIC. Para propiedades físicas que dependen sólo de las diferencias, la aproximación HF + LC parece ser una mejor anternativa que CI.

III.- Corrección de gradientes. Aunque desconocido, el potencial de intercambio-correlación exacto (el de Kohn y Sham) es ciertamente no-local. Esto es, depende de la distribución electrónica en todo el espacio y no solamente del valor de ρ en un punto dado de él. Entoces para ir más allá de la aproximación local pareciera natural el desarrollo de una teoría que involucrase tanto a las derivadas espaciales de ρ así como a la ρ misma. En efecto, hace ya algunos años von Weizsäcker[37] empleó esta idea para efectuar correciones a la energía cinética del gas de electrones Pero recientemente Herman et al[38,39] desarrollaron el método $X_{\alpha\beta}$ en el cual la energía total esta dada por:

$$E_{X\alpha\beta} = E_{X\alpha} - \beta \int \left(\frac{(\nabla \rho_{\uparrow}^2)}{\rho_{\uparrow}^{4/3}} + \frac{(\nabla \rho_{\downarrow}^2)}{\rho_{\downarrow}^{4/3}} \right) dr \quad ,$$

en donde $E_{X\alpha}$ es la energía total de un gas homogéneo de electrones para el cual las interacciones de intercambio estan dadas por la Ec. 19. Y β en un nuevo párametro que toma en cuenta los efectos de las inhomogeneidades de la densidad electrónica *via* las derivadas espaciales de ρ sobre todo el espacio. Entonces las correcciones del método $X_{\alpha\beta}$ pueden ser importantes o cruciales en sistemas en donde existan grandes

inhomogeneidades de la densidad electrónica. Pero este es el caso justamente de átomos, moléculas, metales magnéticos de metales de transición ó de cualquier otro sistema de interés químico.

La ventaja práctica del método $X_{\alpha\beta}$ es que con solamente dos párametros es posible construir un potencial que tome en cuenta las interacciones de intercambio y algunas contribuciones de la correlación electrónica para cualquier elemento de la tabla periódica en cualquier situación física dada. El valor numérico de los párametros α y β es el mismo. α =2/3 y β =0.0025, para todos los elementos químicos. En este sentido α y β son constantes universales. El potencial $X\alpha\beta$ es justamente el que se empleará en la mayoría de los cálculos reportados en esta tésis, este esquema ha sido nuestro *caballo de batalla* en el análisis de la estructura electrónica de una gran variedad de sistemas del bloque *s*, *p*[40,41,42] así como del bloque *d* y/o *f*[43,44]. En nuestro laboratorio hemos encontrado de manera *heurística* que el valor de 0.0025 para β, reproduce bastante bien tanto a los parámetros moleculares de especies en espacio libre[40,41,42] así como a las propiedades electrónicas de cúmulos de metales de transición[43] ó de tierras raras[44] en el seno del cristal. En otra palabras, ciertas propiedades de naturaleza local del estado sólido así como algunos efectos que el entorno líquido[42] ejerce sobre una molécula embebida en él también pueden ser analizados con el método $X\alpha\beta$.

Anteriormente, en H_2[40] y en He_2^{++}[41], hemos comparado nuestros resultados con los de otros métodos así como con el experimento, el acuerdo ha sido razonable. Pero es en los dímeros de metales de transición en donde hemos calibrado recientemente nuestras técnicas para su óptima aplicación en sistemas de mayor complejidad como son los

cúmulos de metales de transición. Particularmente, ha sido en los dímeros de Mo_2[45] y NbIr en donde hemos aprendido como aplicar el método a esta clase de sistemas[46].

En efecto, nuestros resultados para la molécula Mo_2 son de calidad comparable a los obtenidos con otros cálculos a primeros principios tal como el de Goodgame y Goddard III, que emplean la técnica de unión-valencia-generalizad-van der Waals (GVB-vdw)[47]. Estos últimos autores cuestionaban seriamente el empleo de funcionales locales de la densidad en sistemas que involucran átomos de transición. Y el cuestionamiento surgió en este terreno porque en funcionales de la densidad el término de intercambio-correlación se aproxima, para cualquier sistema, por el de un gas homogéneo de electrones . Entonces podría esperarse que este esquema no fuese aplicable en el límite de electrones altamente localizados como es el caso de átomos o moléculas de elementos de transición, en donde además existen grandes inhomogeneidades de la densidad electrónica.

Nuestros cálculos para el estado basal concuerdan razanoblemente bien con los obtenidos por Delley, Freeman y Ellis[48], que también emplearon funcionales locales de la densidad (LD); los resultados con LD comparan mejor con el experimento que los obtenidos con GVB-vdw[47]. Mientras que la aparición de un segundo mínimo en dímeros de metales de transición ha sido confirmada recientemente por cálculos sofisticados dentro del esquema unión-valencia(M-GVB)[49].

Para cúmulos pequeños que consisten de unos cuantos átomos de la serie de transición es posible efectuar cálculos muy sofisticados que incluyen tanto la interación de intercambio así como la correlación

electrónica mediante el empleo de la tecnología Hartree-Fock más interacción de configuraciones (HF + CI). Y ha sido en la molécula diátomica de Cu_2 en donde estas técnicas han llegado a un nivel muy alto[50,51] de sofistificación. En esta misma línea también cabe mencionar los resultados obtenidos en Cu_3[52].

Por otra parte, para cúmulos grandes (A_n) de átomos ligeros de metales alcalinos, se ha explicado la estabilidad que adquieren ciertos tamaños del cúmulo (los números mágicos "n") mediante modelos tipo "jellium"[53]. Pero esta técnica es muy simplista y no permite analizar en detalle efectos magnéticos. Este mismo tipo de cúmulos también ha sido estudiado a nivel Hartree-Fock no-restringido (UHF), y a pesar de mostrar ciertas ventajas sobre otras técnicas, presenta problemas en la convergencia de la energía de cohesión[54].

Las técnicas ab-initio tradicionales resultan ser particularmente difíciles de emplear (al menos por el momento son casi prohibidas) en cúmulos pequeños que consten de unos cuantos átomos de metales de transición (más de tres). Para estas especies resulta más adecuado emplear otro tipo de métodos, también a primeros principios, tales como el esquema de pseudopotenciales[15] o bien las técnicas provenientes de los funcionales de la densidad[16].

En el siguiente capítulo expondremos los resultados que hemos obtenido para algunos cúmulos de níquel y la interacción de estos con hidrógeno átomico y molecular; esto último tratando de modelar algunas coordenadas de reacción para el proceso de la quimisorción. Como hemos mencionado, se usarán técnicas de dispersión múltiple para resolver las ecuaciones de Khon-Sham. Particularmente emplearemos el Método Celular

de Dispersión Múltiple, MCDM-$\chi_{\alpha\beta}$. en una versión desarrollada é implementada en nuestro laboratorio casi totalmente[40,42,43].

REFERENCIAS.

1.- J. P. Borel & J. Buttet (editores) Small Particles and Inorganic Clusters, Surf. Sci. 106 (1981) North-Holland Publishing Company Amsterdam (1981).

2.- T.H. Maugh, Science 219, 474 (1983).

3.- R. L. Whetten, D. M. Cox, D. J. Trevor, and A. Kaldor, Phys. Rev. Lett. 54, 1494, (1985).

4.- S. C. Richtsmeier, E. K. Parks, K. Liu, L. G. Pobo, and S. J. Riley J. Chem. Phys. 82, 3659 (1985).

5.- M. D. Morse, M. E. Geusic, J. R. Heath, and R. E. Smalley, J. Chem. Phys. 83, 2293 (1985).

6.- K.A. Gingerich, Currents Topics in Materials Science, Vol.6, p. 344-462(1980). Editado por E. Kaldis. North-Holland Publishing Company, Amsterdam(1980).

7.- M. Castro. Enlace químico en dímeros de metales de transición. Tesis de Maestría. Facultad de Química, UNAM, México (1984).

8.- M. Moskovits, D. P. DiLella and W. Limm, J. Chem. Phys. 80,626(198).

9.- M. Moskovits and G.A. Ozin(Editores) Cryochemistry. Wiley, New York(1976).

10.- G.A. Ozin, Faraday Symp. Chem. Soc. 14,7-64(1980).
G.A. Thompson, F. Teschler and D.M. Lindsay, J. Chem. Phys. 78,5946(1983).
R.J. Van Zee, C.A. Baumann, S.V. Bhat, and W. Weltner, Jr., J. Chem. Phys. 76,5636(1982).

11.- Magnetic Properties of Low-Dimensional Systems. Springer-Verlag, Berlin Heidelberg 1986. Editado por L.M. Falicov y J.L. Morán-López.

12.- L. E. Klebanoff, S. W. Robey, G. Liu and D. A. Shirley, Phys. Rev. B 30, 1048 (1984).

13.- D. Weller, S. F. Alvarado, W. Gudat, K. Schroder and M. Campagna, Phys Rev. Lett. 54, 1555(1985). S. F. Alvarado, M. Campagna, and H. Hopster, Phys. Rev. Lett. 48, 5, 1768 (1982).

14.- *The Challenge of d and f Electrons*, D. R. Salahub and M. C. Zerner, Eds. Symp. Ser. 394, (1989).

15.- O. A. Novaro in *The Challenge of d and f electrons*, D. R. Salahub and M. C. Zerner, Eds., ACS Symp. Ser. 394, 228 (1989).

16.- Theory and Applications of Density Functionals Approaches to Chemistry. Springer-Verlag, Columbus, 1991. Editado por J. K. Labanowsky y J. W. Andzelm.

17.- D. R. Salahub, Adv. Chem. Phys. 69, 447 (1987).

18.- P. Hohenberg y W. Kohn, Phys. Rev. 136, B864 (1964).

19.- W. Khon y L.J. Sham, *Phys. Rev.* 140, A1133 (1965).

20.- P. Drude, *Annalen der Physik I*, 566 y ibid *III*, 369 (1900).

21.- N.W. Ashcroft y N.D. Mermin, Solid State Physics. Holt, Rinehart y Winston, Philadelphia 1976.

22.- N. H. March, *Self-Consistent Fields in Atoms - Hartree and Thomas Fermi Atoms*, Pergamon, New York, 1975.

23.- U. von Barth y L. Hedin, *J. Phys. C: Solid State Phys.*, 5, 1629 (1972).

24.- J. C. Slater, *Adv. Quantum Chem.*, 6, 1 (1972). *The Self Consistent Field for Molecules and Solids*, Vol. 4, MacGraw-Hill, New York, 1974.

25.- R. Gaspar, *Acta Phys. Acad. Sci. Hung.*, 3, 263 (1954).

26.- J. C. Slater, *Phys. Rev.* 81, 385 (1951).

27.- O. Gunnarsson y B. I. Lundqvist, *Phys. Rev. B*, 13, 4274 (1976).

28.- J.F. Janak, V.L. Moruzzi y A.R. Williams, *Phys. Rev. B* 12, 1257 (1976).

29.- S.H. Vosko, L. Wilk y M. Nusair, *Can. J. Phys.* 58, 1200 (1980).

30.- J.P. Perdew y A. Zunger, *Phys. Rev. B*, 23, 5048 (1981).

31.- J. P. Perdew, *Chem Phys. Lett.*, 64, 127 (1979).

32.- H. Stoll, E. Golka, and H. Preuss, *Theor. Chim. Acta*, 49, 143 (1978).

33.- Y. S. Kim and R. G. Gordon, *J. Chem. Phys.*, 60, 1842 (1974).

34.- H. Stoll, C.M.E. Pavlidou and H. Preuss, *Theor. Chim. Acta*, 49, 143 (1978).

35.- S. H. Vosko and L. J. Wilk, *J. Phys. B: At. Mol. Phys.*, 7, 3687 (1983).

36.- E. Fermi and E. Amaldi, *Accad. Ital. Rome*, 6, 119 (1934).

37.- C. F. von Weizäcker, *Z. Phys.* 96, 431 (1935).

38.- F. Herman, J. P. Van Dyke and I. B. Ortenburger, Phys. Rev. Lett. 22, 807 (1969).

39.- F. Herman, I. B. Ortenburger and J. P. Van Dyke, *Int. J. Quantum Chem.*, S3, 827 (1970).

40.- A. Garritz, J. L. Gázquez, M. Castro, and J. Keller, Int. J. Quantum Chem. 15, 731 (1979).

41.- M. Castro, J. Keller and O. N. Ventura, J. Chem. Phys. 77, 6348 (1982).

42.- M. Castro, J. Keller and P. Rius, Hyperfine Interact. 12, 261 (1982).

43.- J. Keller, M. Castro and A.L. de Paoli, J. Appl. Phys. 53, 8850 (1982).

44.- J. Keller, M. Castro, and C. Amador, *Physica* 102B, 129 (1980).

45.- M. Castro, J. Keller, and P. Mareca, Int. J. Quantum Chem., Quantum Chem. Symp. 15, 429 (1981).

46.- M. Castro, J. Keller, and P. Mareca, Int. J. Quantum Chem. 39, 000 (1991).

47.- M. M. Goodgame and W. A. Goddard III, Phys. Rev. Lett. 48, 135 (1982).

48.- B. Delley, A. J. Freeman and D. E. Ellis, Phys. Rev. Lett. 50, 488 (1983).

49.- M. M. Goodgame and W. A. Goddard III, Phys. Rev. Lett. 54, 661 (1985).

50.- C. W. Bauschlicher, Jr., S. P. Walch and P. E. M. Siegbahn, J. Chem. Phys. 76, 6015 (1983)

51.- M. Pelissier, J. Chem. Phys. 75, 775 (1981).

52.- G. del Conde, P. S. Bagus, and O. Novaro, Phys. Rev. B 25, 7843 (198).
S. P. Walch and B. C. Laskowski, J. Chem. Phys. 84, 2734 (1986).

53.- W. D. Knight, K. Clemenger, W. A. de Heer, W. A. Saunders, M. Y. Chou, and M. L. Cohen, Phys. Rev. Lett. 52, 2141 (1984).

54.- J. García-Prieto, G. del Conde, M. Galván, and O. Novaro, Phys. Rev. 30, 1030 (1984).

Local Electronic Structure of Magnetic fcc Palladium.

Miguel Castro

Sección de Química Teórica, Facultad de Química,
Universidad Nacional Autónoma de México,
Delegación Coyoacán, 04510 México D.F., México.

PACS numbers: 71.70.Gm, 73.20.Hb, 75.50.Cc.

Abstract.

We apply the multiple-scattering cluster-in-condensed-matter technique together with local density exchange correlation potentials to study the electronic structure of a single palladium atom embedded in bulk palladium, both in the nonmagnetic phase and in the ferromagnetic environment generated when the system is expanded. From the results the behavior of the *s*, *p*, and *d* orbitals is analyzed as a function of the palladium *fcc* lattice parameter, *a*. In fact, a magnetic phase occurs when *a* has increased about 5 % above the equilibrium lattice constant where spin polarization is compensated. Whereas in magnetic palladium, the magnetic moment, μ = 0.356 spins per atom, and the exchange splitting, δE_{ex} = 0.18 *eV*, gives intra-atomic exchange interactions, $U^{d-d} = \delta E_{ex}/\mu \cong 0.51$ *eV per spin*, of the same strength as in the isoelectronic and isostructural ferromagnetic nickel, $U^{d-d} \cong 0.54$ *eV per spin* (μ = 0.54 *spa* and δE_{ex} = 0.29 eV), computed with the same methodology. In palladium and nickel the *s*- and p-electrons show a small spin-polarization, opposite to the localized magnetization built up by the d-wavefunctions, whose chemical bonding behavior exhibits a similar pattern in both systems. This last constitutes an evidence in favor of a ferromagnetic state in palladium, which is corroborated by total energy calculations: in our approach the ferromagnetic state is $\cong$ 1.5 *mRy* and $\cong$ 2.0 *mRy* deeper than the antiferromagnetic and paramagnetic states, respectively.

Introduction.

A basic theoretical problem is the study of the existence of a ferromagnetic state in terms of modern electronic structure. Here, the *ab-initio* self-consistent band structure techniques have been successfully applied and provided a quantitative understanding of many ground-state properties in iron, cobalt and nickel[1]. The accuracy of such techniques is such that it is now possible to take the lattice parameter as an input variable, and to determine its equilibrium value for a given structure. In this way it has been predicted that the normally paramagnetic face-centered-cubic palladium[2] should become magnetic when it is expanded about five per cent[2,3,4]. This was expected encouragely given that palladium is isoelectronic and isostructural to ferromagnetic nickel and since the degree of the *s-d* hybridization depends on the lattice constant strongly.

On the other hand, magnetic properties of a highly local character may also be analyzed in a real space formalism by means of calculations for a cluster embedded in the bulk of the material[5]; in this scheme the electronic structure for the analysis of those properties is readily extracted, and the theoretical explanation of them is given in terms of quantum chemical concepts which provides complementary information, and in some cases a new interpretation, to that commonly given for solid state phenomena by means of the reciprocal-space methodology.

In this paper we calculate the electronic structure of a single palladium atom in two cases: embedded in the bulk of the nonmagnetic phase of palladium at the *fcc* lattice equilibrium parameter, and in the ferromagnetic environment generated when the *fcc* structure is allowed to expand. We also present some results for *fcc* ferromagnetic nickel in order to discuss more widely the nature of the *fcc* Pd magnetic state. Besides we will report some complementary information to that obtained previously in *fcc* Pd by means of the band theory methods[2,3,4] .

Our spin-polarized calculations are carried out by means of a simple algorithm, in the real space formalism, that allows easily the computation of the local electronic structure of ferromagnetic materials[5] . For this purpose an atom embedded in the crystal is studied self-consistently in a spin polarized environment representing the ferromagnetic bulk of the material. Our all electron calculations are performed with multiple scattering techniques[5,6] combined with local spin density functionals for the exchange-correlation effects in the way explained below.

Computational Procedure.

A) Free palladium atomic densities were computed self-consistently in the $4d^{10-x-y}\ 5s^{x}\ 5p^{y}$ atomic configurations. Just at the beginning there were no $5s$ nor $4p$ electrons. These atomic spin-polarized calculations are performed with a modified version of a relativistic self-consistent field method[7]. The modifications include the use of the α-β exchange-correlation potential[8] and the possibility of minimizing the

total energy as a function of the fractional occupation of the valence levels. The electronic spin-polarized charge density is the main product of this atomic step.

B) The environment of a given atom in the bulk material is represented by a potential which takes into account the contribution of the first six nearest layers of neighbor atoms. This one-electron crystal potential is built-up from the superposition of atomic charge densities, in which only the spherically symmetric part is kept. Starting from this density the Poisson equation is solved for the Coulombic part and the exchange-correlation contribution is approximated in the α-β scheme[8].

In the real-space formalism the atomic cell radius R_c, corresponds to that of the volume per atom sphere. For *fcc* palladium we have started the calculations with a zero-temperature lattice constant of 7.32961 *a. u.*[2], equivalent to a palladium sphere radius of 2.8944 *a. u.* The total number of electrons inside the Wigner-Seitz sphere is equal to the atomic number Z. In the single site-approximation for the crystal potential, a search for the set of resonances was carried out by means of the Cellular Multiple Scattering $X_{\alpha\beta}$ technique[5,6]. The potential outside the central region was kept frozen. See figure 1 for a representation of the crystal potential. The purpose of our study is to obtain more understanding of the way the condensed matter boundary conditions for the one-electron wavefunctions act on a group of atoms to promote a magnetic state in it.

C) A charge density for the central cell was constructed in a band-like picture fashion: all *s*, *p*, *d*, *f* and *g* spin-orbitals with eigenvalues less than an E_{max} are occupied with fractional occupation numbers

(determined below); E_{max} is that energy for which the total number of electrons inside the cell, with eigenvalues $\varepsilon_i \leq E_{max}$, is equal to Z.

In the multiple scattering techniques, the local density of states for the atomic species i, at energy E, is given by integration over cell i of the diagonal elements of the imaginary part of Green's function[5,6]

$$-(1/\pi)\int_0^{R_c} dr \langle r|\,\mathrm{Im}\; G^+(E)|r\rangle = \int_0^{R_c} \rho(r;E)\, dr \quad . \qquad (1)$$

The G^+ matrix of the system is given in terms of the free electron Green's function G_0^+ and the array of the single site scattering matrices K, for stationary wave boundary conditions. G^+ can be expressed in a supermatrix angular momentum representation ($\tilde{G}^+$) as

$$\tilde{G}^+_{iL,jL'} = \sum_{kL''} \tilde{G}^+_{0iL,kL''} \left[\left(\tilde{I} - \tilde{G}_0^+ \tilde{K} \right)^{-1} \right]_{kL'',jL'} \quad , \qquad (2)$$

L is the ordered pair (l,m) and i,j,k denote scatterer atoms. The radial local density of states can be written in terms of the supermatrix as

$$\rho_l(r';\, E) = -4 \langle\langle r'|\,\mathrm{Im}\; G^+(E)|r'\rangle\rangle_{sp} \quad ,$$

$$= -4 \sum_L R_l^2(r';E)\; \mathrm{Im}\; G^+_{Ll,Ll} \quad , \qquad (3)$$

where sp = spherical average; $r' = |r'| = |r-r'|$; $R_l(r';\, E)$ are the

solutions for energy E of the radial Schrodinger equation for scatterer i in the self-consistent atomic potential with the boundary condition:

$$R_l(r_c'; E) = j_l(\kappa r_c')\cos\eta_l - n_l(\kappa r_c')\sin\eta_l \quad , \qquad (4)$$

where $E = \kappa^2$; j_l and n_l are the Bessel and Neumann spherical functions, modulated by $cos\eta_l$ or $sin\eta_l$, respectively; η_l is the phase shift of the partial scattered wave, with angular momentum index l.

The potentials are computed from the charge densities by solving Poisson equation and using the exchange $X_{\alpha\beta}$ technique[8]. In the self-consistent procedure for the central (cluster) region the eigenstates were divided into core and conduction bands. We make the simplification of treating inner orbitals as core electrons. The conduction band itself was divided into s, p, d, f, and g cluster resonances for which the integration in Eq. (1) gives fractional occupation numbers. All valence orbitals with eigenvalues less than E_{max} are occupied with that non-integer occupation numbers. The crystal potential outside the central cell was kept frozen during the SCF process and at the end of this step the central cell has acquired a different electronic arrangement from that of the atoms in the frozen layers. Just at the end of this step are determined the x and y electronic population parameters, resolved by angular momentum components for each spin. With these new spin-orbital occupations the atomic calculation (A) is repeated, a new crystal model potential (B) is constructed and the electronic structure in the central region is recalculated as in (C). After three A → B → C cycles the electronic

population parameters of the step A have converged to the occupation numbers obtained in C: the electronic arrangement of the central atom is equal to that of the atoms in the frozen environment. At this point E_{max} defines the Fermi level (ε_f), of the system.

Results.

The self-consistent eigenvalues, ε_i, of the valence band together with the occupation numbers (n_i, given by Eq. 1), for both occupied (n_i = Ocupp.) and empty levels, the accumulated charge of each spin ($\uparrow$ = majority-spin, $\downarrow$ = minority-spin) and the total accumulated charge ($\uparrow + \downarrow$) up to the Fermi level are reported in table 1 for nonmagnetic palladium (NM-Pd), a = 7.329 *a. u.*, and in table 2 for magnetic palladium (M-Pd), a = 7.720 *a. u.* For comparison, a similar information is reported in table 3 for ferromagnetic *fcc* nickel at a fixed lattice constant of 6.6541 *a. u.*[9]. The tables contains only the more important information. In the three cases the conduction band may be partitioned in three main pieces:

i) The set of eigenvalues contained in the ranges: -4.1 Ry $\leq \varepsilon_i \leq -1.8$ Ry for NM-Pd, -4.4 Ry $\leq \varepsilon_i \leq -2.2$ Ry for M-Pd, and -4.2 Ry $\leq \varepsilon_i \leq -1.7$ Ry for FM-Ni belong to wavefunctions that are centered at the atoms in the frozen layers and present very small contributions to the local density of states in the central cell. These sets are not showed in the tables.

ii) The *s*, *p*, and *d* bands of the central cells emerge at: -1.31 Ry $\leq \varepsilon_i \leq -0.93$ Ry for NM-Pd, -1.87 Ry $\leq \varepsilon_i \leq -1.50$ Ry for M-Pd, and -1.71 Ry $\leq \varepsilon_i \leq$

-1.51 Ry for FM-Ni. Also, next to these levels the f and g spin orbitals begin to appear but with smaller populations.

iii) The genuine wavefunctions of the central atom are contained at: -0.61 Ry $\leq \varepsilon_i \leq \varepsilon_f = -0.25$ Ry for NM-Pd, -1.16 Ry $\leq \varepsilon_i \leq \varepsilon_f = -0.47$ Ry for M-Pd, and -0.99 Ry $\leq \varepsilon_i \leq \varepsilon_f = -0.50$ Ry for FM-Ni. These orbitals shows high contributions to the local density of states in the central region, which produces a high sharp structure near the top of the bands in the three cases; a similar pattern has been found for this kind of systems by means of the band-theoretical techniques. Almost all the physics of the problem is given by this set of wavefunctions, with some of them empty, partially occupied or totally filled, depending on the extracted information about the system. We discuss below the ground states of non-magnetic palladium, magnetic palladium and ferromagnetic nickel.

Discussion.

Our electronic structure for fcc Pd at the lattice equilibrium parameter gives a null magnetization: the occupation numbers of the up- and down- spin orbitals, of each angular momentum component, are compensated; see table 1. In this paramagnetic phase the highest occupied levels of each spin are of d character: the t_{2g} orbitals of a cubic symmetry with large occupation numbers, 4.329 for each one, *i. e.* in nonmagnetic palladium there is a high density of states (of d-type) at the Fermi level, which agrees qualitatively with some energy-band studies[2,10].

In *fcc* Pd a magnetic phase occurs when *a* increases by 5.3% above the lattice equilibrium parameter. In our approach this is the point at which the spin compensation of the potentials has broken down. Without including spin-orbit effects the magnetic phase transition has been observed in band theory when the lattice constant is expanded by 5 to 6%[2,3,4]. At *a* = 7.735 *a. u.*, Chen et al[2] obtains a magnetic moment of 0.31 *spa* which is close to our value of 0.35 *spa* for *fcc* Pd at *a* = 7.72 *a. u.*, see table 2.

The overall SCF electronic structure for *fcc* Ni displayed in table 3 produces a total magnetization of 0.539 *spa*, which is in essence of *d*-character and close to the experimental result of 0.56 *spa*[11]. In nickel the e_g and t_{2g} *d*-orbitals, near the Fermi energy, together give a magnetization of 0.548 *spa*, a figure slightly larger than the total quoted above, which implies an opposed small magnetization of the *s* and *p* electrons. In fact, in each couple (spin-up and spin-down) of *s* and *p* orbitals in the occupied conduction band, the magnetization is small and negative, see table 3.

Our SCF electronic structure for *fcc* Ni predicts a nonmagnetic state for *fcc* copper (in a rigid band model scheme) : if the *d*-minority orbital at the Fermi level would be totally filled with 1.82 *e* instead of 1.31 e that acquires in the ferromagnetic ground state (the occupation number of his counterpart *d*-majority orbital is of 1.52), the magnetization of the e_g levels, -0.30 *spa*, would cancel exactly the positive magnetization of the t_{2g} *d*-levels immediately below, with the remaining electrons filling the *s* and *p* empty orbitals, see table 3.

At *a* = 7.72 a.u., the total energy of the *fcc* Pd magnetic

state, -9875.8175 *Ry*, is only ≅ 1.5 *mRy* deeper than the nonmagnetic state total energy; this last property was computed assigning equal occupation numbers in each couple of spin-up and spin-down orbitals. Whereas, the total energy for the antiferromagnetic state was calculated exchanging the spin-up and spin-down potentials of the frozen environment, keeping the same occupation numbers of the magnetic state (the set n_i given in table 2); in this way it was obtained -9875.8120 *Ry* for the AF state. These crude calculations, for the NM and AF states, indicates that the magnetic order of the *fcc* Pd is ferromagnetic, at the lattice constant of 7.72 *a. u.*.

On the other hand, the energy of an external magnetic field necessary to induce a first order phase transition from the paramagnetic to the ferromagnetic state, in palladium, is of 1.3 *mRy*[10], with a resulting magnetic moment of 0.20 *spa*[10].

In *fcc* Ni the e_g and t_{2g} orbitals experiments *d*-exchange separations of 0.31 *eV* and of 0.26 *eV*, respectively, see table 3. On the other hand, Eastman et al[12] have reported an exchange splitting of 0.30 *eV* for nickel . Our total population numbers for the nickel majority and minority d-bands are of 4.71 and of 4.16, respectively, these values are close to those obtained by Langlais and Callaway[13], 4.78 and 4.22.

However, in magnetic palladium the spin-up and spin-down potentials are splitted to a lesser extent than in ferromagnetic nickel. The highest exchange splittings, in M-Pd, occur for the levels just contained in *range iii*: -1.16 Ry ≤ $\varepsilon_i \leq \varepsilon_f$ = -0.47 Ry. Here the e_g and t_{2g} occupied *d*-orbitals suffer separations of 8 mRy (0.11 *eV*) and 18.3 *mRy* (0.25 *eV*), respectively. Whereas the *s* and *p* wavefunctions, nearer the

Fermi energy, are splitted by 6 *mRy*; see table 2.

Using our average exchange splittings (δE_{ex}= 0.18 *eV* for Pd and 0.29 *eV* for Ni) and magnetizations (μ = 0.35 *spa* and 0.54 *spa* for Pd and Ni, respectively) we find that the intra-atomic exchange interactions, namely $U^{d-d} = \delta E_{ex} / \mu$, in palladium (U = 0.51 *eV per spin*) are of the same strength than the intra-atomic exchange interactions in ferromagnetic nickel (U^{d-d} = 0.54 *eV per spin*).

We have also performed calculations using the spin-dependent exchange-correlation potential of von Barth and Hedin[14] (vBH). Our results for nickel are: δE_{ex} = 0.57 *eV* (0.042 Ry) and μ = 0.58 *spa*, which gives an intra-atomic exchange interaction, U^{d-d}, of 0.98 *eV*. Except for the case of the magnetization, it is quite evident that δE_{ex} and U^{d-d} are somehow dependent on the exchange-correlation model but in both cases, either $X_{\alpha\beta}$ or vBH approaches, our results are lower than those of band theory for nickel[15]: δE_{ex}= 0.63 *eV*, μ = 0.58 *spa* and U^{d-d} = 1.09 *eV per spin*.

The $X_{\alpha\beta}$ potential regularly gives good magnetizations and not too high exchange-splittings in highly localized *d* electron systems. For instance in magnetic impurities of iron in palladium the present model gives a moment of 3.32 *spa* on the iron site[16], which agree with the experimental value[17], 3.50 $\pm$ 0.4 *spa*, and with results of other methods: 3.54 *spa*[18], 3.24 *spa*[18], and 3.45 *spa*[19]. In this last paper a value of δE_{ex} was not estimated. Our model gives: δE_{ex}= 1.74 *eV* and U^{d-d} = 0.52 *eV*[16]. In another giant-moment system, iron impurities in rubidium, it was calculated on the iron site[20]: μ = 3.12 *spa*, δE_{ex}= 2.42 *eV*, and U^{d-d} = 0.78 *eV*.

Most of the cited results[2,3,15,19,20] were obtained with an exchange-correlation vBH model in some chosen parameterization[1,21]. Rigorously, in the $X_{\alpha\beta}$ model there is no electronic-correlation; all its virtues are derived from an account of the exchange interactions and from a proper description of the effects of inhomogeneities of the electronic charge distribution, taken into account by the density gradients in the β part of the $X_{\alpha\beta}$ scheme[8].

On the other hand, the experimental exchange-splittings and Bohr-magneton data give an almost constant U^{d-d}, $\cong$ 0.6 - 0.7, for Fe, Co and Ni ferromagnetic materials[12]. Actually this narrow energy range has not been attained so far by the first-principles approaches[12]. In its actual states the $X_{\alpha\beta}$ model underestimates while the vBH models overestimates the exchange-splittings. Nevertheless, the present results stress the importance of the density gradients, along with the density itself, for obtaining a reasonable estimation of the magnetic properties in highly localized d electron systems in condensed matter.

Additionally, the boundary conditions we use in the model study of embedded clusters accounts properly for chemical bonding effects (electron pairing) which compensate the usually high spin-enhancement (magnetization) due to the LSD exchange-correlation potential and explains, to some extent, the not too high exchange-splittings of nickel and palladium in our results . This may be more clearly seen in the analysis of the relevant electronic states presented bellow.

In figure 2 is presented the radial distribution function for the highest occupied d-wavefunctions of majority spin in magnetic

palladium, the levels of table 2 at $\varepsilon_i = -0.972$ with $n_i = 1.43$, and at $\varepsilon_i = -0.767$ with $n_i = 2.39$, which corresponds, respectively, to the e_g and t_{2g} orbitals of a cubic symmetry. The next main features are appreciated from that figure. The e_g orbital is almost entirely localized in the palladium atomic sphere. Whereas the t_{2g} orbital shows a strong chemical bonding behavior between the central and its first nearest neighbors: the *d*-electronic charge is accumulated in the internuclear region among these two kinds of atoms.

Similarly, in figure 3 is presented the radial distribution function for the e_g and t_{2g} wavefunctions of majority spin in ferromagnetic *fcc* nickel, the levels of table 3 at $\varepsilon_i = -0.57$ Ry with $n_i = 1.56$ and at $\varepsilon_i = -0.75$ Ry with $n_i = 3.10$. The behavior of these wavefunctions follows the same pattern to that of the magnetic *fcc* palladium d-orbitals.

Conclusions.

Combining the multiple-scattering techniques together with density-functional exchange correlation potentials, we have designed and applied an algorithm that allows easily the computation of the local electronic structure of atoms and clusters embedded in magnetic materials. Our results are not far away of those obtained with the more sophisticated band theory techniques. The intra-atomic exchange interactions, U^{d-d}, the chemical bonding behavior displayed by the d-wavefunctions as well as the total energy calculations for the

magnetic states, points towards a possible occurrence of a ferromagnetic state in expanded *fcc* palladium, the electronic structure of this system shows strong similarities with those of the usually ferromagnetic materials, *e.g. fcc* nickel. Although more accurate calculations are needed for addressing a definitve answer to this question.

Here, we have presented results of pure ferromagnetic materials but, as mentioned, this methodology is a powerful tool for the theoretical analysis of dilute magnetic alloys[16]. The algorithm also can be applied to the study of metastable phases, *e. g.* ferromagnetic *bcc* cobalt[22].

Acknowledgments.

Financial support for this research was provided by DGAPA–UNAM under Project: IN–10–40–89. We wish to thank all the staff of the computer center at DGSCA–UNAM.

References.

1.- V. L. Moruzzi, J. F. Janak and A. R. Williams, Calculated Electronic Properties of Metals (Pergamon, New York, 1978).

2.- H. Chen, N. E. Brener, and J. Callaway, Phys. Rev. B40, 1443 (1989).

3.- V. L. Moruzzi and P.M. Marcus, Phys. Rev. B39, 471 (1989).

4.- L. Fritsche, J. Noffke, and H. Eckardt, J. Phys. F17, 943 (1987).

5.- J. Keller, M. Castro, and A. L. de Paoli, J. Appl. Phys. 53, 8850 (1982).

6.- M. Castro, J. Keller, and P. Rius, Hyperfine Interactions 12, 21 (1982).

7.- D. Liberman, J. T. Waber, and D. T. Cromer, Phys. Rev. 137, 27, (1965).

8.- F. Herman, J. P. Van Dyke, and I. B. Ortenburger, Phys. Rev. Lett. 22, 807 (1969).

9.- N. W. Ashcroft and N. D. Mermin, *Solid State Physics*, Holt-Saunders International Editions, Japan, 1971.

10.- T. Jarlborg and A. J. Freeman, Phys. Rev. B23, 3577 (1981).

11.- H. Dannan, *et al*, J. Appl. Phys. 39, 669 (1968).

12.- D. E. Eastman, F. J. Himpsel and J. A. Knapp, Phys. Rev. Lett. 44, 95 (1980).

13.- J. Langlais and J. Callaway, Phys. Rev. B5, 124 (1972).

14.- U. von Barth and L. Hedin, J. Phys. C 5, 1629 (1972).

15.- C. S. Wang and J. Callaway, Phys. Rev. B 15, 298 (1977).

16.- A. Rodriguez and J. Keller, J. Phys. F11, 1423 (1981).

17.- G. G. Low and T. M. Holden, Proc. Phys. Soc. 89, 119 (1966).

18.- B. Delley, D. E. Ellis, and A. J. Freeman, J. Magn. Magn. Mat 30, 71 (1982).

19.- A. Oswald, R. Zeller, and P. H. Dederichs, Phys. Rev. Lett. 56, 1419, (1986).

20.- M. E. McHenry, J. M. MacLaren, D. D. Vvedensky, M. E. Eberhart, and M. L. Prueitt, Phys. Rev B 40, 10111 (1989).

21.- L. Hedin and B. I. Lundqvist, J. Phys. C 4, 2064 (1971).

22.- M. Castro, V. Soria, and F. Estrada, in: Theory and Applications of Density Functionals Approaches to Chemistry. Springer-Verlag, Columbus, 1991. J. K. Labanowsky and J. W. Andzelm, Eds. In press.

Table 1.- Eigenvalues, ϵ_i, and occupation numbers, n_i, for Pd(fcc). The sum of the accumulated charge for each spin at the Fermi energy is equal to the number of valence electrons per atom; the difference gives a null magnetization.

Orbital	$\epsilon_i(Ry)$	n_i	Occup.	Total ↑	Total ↓	↑ + ↓
s^1	−4.0313	0.00035	0.00035	0.00035		0.00035
s^1	−4.0313	0.00035	0.00035		0.00035	0.00070
p^1	−3.9541	0.00184	0.00184	0.00219		0.00254
p^1	−3.9541	0.00184	0.00184		0.00219	0.00438
d^1	−3.8001	0.00117	0.00117	0.00339		0.00555
d^1	−3.8001	0.00117	0.00117		0.00336	0.00672
f^1	−3.5710	0.00110	0.00110	0.00446		0.00782
f^1	−3.5710	0.00110	0.00110		0.00446	0.00892
s^1	−3.3346	0.00003	0.00003		0.00449	0.00895
s^1	−3.3346	0.00003	0.00003	0.00449		0.00898
p^1	−3.3096	0.00002	0.00002		0.00451	0.00900
p^1	−3.3096	0.00002	0.00002	0.00451		0.00902
g^1	−3.2704	0.00086	0.00086	0.00537		0.00988
g^1	−3.2704	0.00086	0.00086		0.00537	0.01074
d^1	−3.2597	0.00054	0.00054		0.00546	0.01083
d^1	−3.2597	0.00054	0.00054	0.00543		0.01089
f^1	−3.1848	0.00016	0.00016		0.00562	0.01105
f^1	−3.1848	0.00014	0.00014	0.00557		0.01119
g^1	−3.0826	0.00005	0.00005	0.00567		0.01124
g^1	−3.0826	0.00005	0.00005		0.00562	0.01129
s^1	−2.0591	0.00005	0.00005		0.00572	0.01134
s^1	−2.0591	0.00005	0.00005	0.00567		0.01139
p^1	−2.0103	0.00010	0.00010		0.00582	0.01149
p^1	−2.0103	0.00010	0.00010	0.00577		0.01159
d^1	−2.0031	0.00090	0.00090		0.00672	0.01247
d^1	−2.0031	0.00092	0.00092	0.00669		0.01341
f^1	−1.9481	0.00006	0.00006		0.00678	0.01347
f^1	−1.9481	0.00006	0.00006	0.00675		0.01353
g^1	−1.8758	0.00003	0.00003		0.00681	0.01356
g^1	−1.8758	0.00003	0.00003	0.00678		0.01359
s^1	−1.3119	0.00625	0.00625	0.01303		0.01984
s^1	−1.3119	0.00625	0.00625		0.01306	0.02609
p^1	−1.2680	0.00975	0.00975	0.02278		0.03584
p^1	−1.2680	0.00975	0.00975		0.02281	0.04559
d^1	−1.1875	0.01186	0.01186	0.03164		0.05745
d^1	−1.1875	0.01186	0.01186		0.03167	0.06931
f^1	−1.0731	0.00391	0.00391	0.03855		0.07322
f^1	−1.0731	0.00392	0.00392		0.03859	0.07714
g^1	−0.9307	0.00163	0.00163	0.04018		0.07877
g^1	−0.9307	0.00163	0.00163		0.04022	0.08040
s^1	−0.6088	0.08554	0.08554	0.12572		0.16594
s^1	−0.6088	0.08554	0.08554		0.12576	0.25148
p^1	−0.5384	0.07483	0.07483	0.20055		0.32631
p^1	−0.5384	0.07483	0.07483		0.20059	0.40114
d^1	−0.4742	0.28039	0.28039	0.48094		0.68153
d^1	−0.4742	0.28038	0.28038		0.48097	0.96191
f^1	−0.3817	0.01033	0.01033	0.49127		0.97225
f^1	−0.3817	0.01033	0.01033		0.49130	0.98257
s^1	−0.3132	0.17645	0.17645	0.66772		1.15902
s^1	−0.3132	0.17645	0.17645		0.66775	1.33547
g^1	−0.2867	0.00305	0.00305	0.67078		1.33853
g^1	−0.2867	0.00305	0.00305		0.67078	1.34159
d^1	−0.2528	4.32921	4.32921	5.00000		5.67078
d^1	−0.2528	4.32921	4.32921		5.00000	10.00000
p^1	−0.1662	0.37644				
p^1	−0.1662	0.37645				
s^1	−0.0038	0.00000				
s^1	−0.0038	0.00000				

Table 2.- Eigenvalues, ϵ_i, and occupation numbers, n_i, for Pd(fcc). The sum of the accumulated charge for each spin at the Fermi energy is equal to the number of valence electrons per atom; the difference gives a magnetization of 0.35 spa.

Orbital	ϵ_i(Ry)	n_i	Occup.	Total ↑	Total ↓	↑ + ↓
s^1	−4.3822	0.00033	0.00033	0.00033		0.00033
s^1	−4.3757	0.00033	0.00033		0.00033	0.00066
d^1	−4.1756	0.00108	0.00108	0.00141		0.00174
d^1	−4.1690	0.00108	0.00108		0.00141	0.00283
f^1	−3.9705	0.00100	0.00100	0.00242		0.00383
f^1	−3.9640	0.00100	0.00100		0.00242	0.00483
g^1	−3.6996	0.00079	0.00079	0.00321		0.00563
g^1	−3.6931	0.00079	0.00079		0.00321	0.00642
s^1	−3.5386	0.00015	0.00015	0.00339		0.00657
s^1	−3.5321	0.00003	0.00003		0.00324	0.00660
p^1	−3.5172	0.00007	0.00007	0.00345		0.00667
p^1	−3.5107	0.00005	0.00005		0.00329	0.00672
d^1	−3.4721	0.00578	0.00578	0.00881		0.01210
d^1	−3.4659	0.00207	0.00207		0.00506	0.01476
f^1	−3.4054	0.00081	0.00081	0.00962		0.01557
f^1	−3.3989	0.00416	0.00416		0.01011	0.01973
g^1	−3.3158	0.00173	0.00173	0.01134		0.02146
g^1	−3.3093	0.00000	0.00000		0.01017	0.02152
s^1	−2.4453	0.00016	0.00016	0.01150		0.02168
s^1	−2.4392	0.00015	0.00015		0.01033	0.02183
p^1	−2.4275	0.00026	0.00026	0.01176		0.02209
p^1	−2.4213	0.00026	0.00026		0.01059	0.02235
d^1	−2.3924	0.00023	0.00023	0.01200		0.02258
d^1	−2.3863	0.00023	0.00023		0.01082	0.02281
f^1	−2.3409	0.00011	0.00011	0.01210		0.02292
f^1	−2.3348	0.00010	0.00010		0.01092	0.02302
g^1	−2.2737	0.00010	0.00010	0.01220		0.02312
g^1	−2.2677	0.00009	0.00009		0.01100	0.02321
s^1	−1.8677	0.01041	0.01041	0.02261		0.03302
s^1	−1.8609	0.01036	0.01036		0.02137	0.04398
p^1	−1.8281	0.01464	0.01464	0.03725		0.05862
p^1	−1.8213	0.01458	0.01458		0.03595	0.07320
d^1	−1.7541	0.02485	0.02485	0.06210		0.08805
d^1	−1.7474	0.02342	0.02342		0.05936	0.12146
f^1	−1.6486	0.00516	0.00516	0.06727		0.12663
f^1	−1.6420	0.00514	0.00514		0.06450	0.13177
g^1	−1.5157	0.00206	0.00206	0.06933		0.13383
g^1	−1.5091	0.00205	0.00205		0.06656	0.13589
s^1	−1.1569	0.21370	0.21370	0.28302		0.34958
s^1	−1.1503	0.21375	0.21375		0.28041	0.56334
p^1	−1.0675	0.28078	0.28078	0.57281		0.85312
p^1	−1.0605	0.29043	0.29043		0.57074	1.14355
d^1	−0.9716	1.43151	1.43151	2.00432		2.57506
d^1	−0.9636	1.35112	1.35112		1.92186	3.92618
f^1	−0.8441	0.03873	0.03873	2.04305		3.96491
f^1	−0.8379	0.03840	0.03840		1.99026	4.00331
s^1	−0.7840	0.12215	0.12215	2.16518		4.12544
s^1	−0.7791	0.12112	0.12112		2.08138	4.20656
d^1	−0.7671	2.39456	2.39456	4.55974		6.64113
d^1	−0.7588	2.40971	2.40971		4.49110	9.05083
g^1	−0.7371	0.00815	0.00815	4.56789		9.05898
g^1	−0.7310	0.00808	0.00808		4.49918	9.06706
p^1	−0.7023	0.32307	0.32307	4.89096		9.39013
p^1	−0.6971	0.32369	0.32369		4.82227	9.71322
d^1	−0.4725	1.36777	0.28677	5.17773		10.00000
d^1	−0.1611	1.99241				
f^1	−0.3177	0.35383				
f^1	−0.3112	0.35419				
s^1	−0.1665	0.22490				
s^1	−0.1638	0.21901				
p^1	−0.1281	0.19718				
p^1	−0.1262	0.18020				

Table 3.- Eigenvalues, ϵ_i, and occupation numbers, n_i, for Ni(fcc). The sum of the accumulated charge for each spin at the Fermi energy is equal to the number of valence electrons per atom; the difference gives a magnetization of 0.54 spa.

Orbital	$\epsilon_i(Ry)$	n_i	Occup.	Total ↑	Total ↓	↑ + ↓
$s^{\uparrow}$	−4.1919	0.00125	0.00125	0.00125		0.00125
$s^{\downarrow}$	−4.1770	0.00127	0.00127		0.00127	0.00252
$p^{\downarrow}$	−4.0978	0.00117	0.00117	0.00442		0.00569
$p^{\uparrow}$	−4.0830	0.00321	0.00321		0.00118	0.00890
$d^{\downarrow}$	−3.9133	0.00158	0.00158	0.00800		0.01248
$d^{\uparrow}$	−3.8985	0.00361	0.00361		0.00809	0.01609
$f^{\uparrow}$	−3.6494	0.00262	0.00262	0.01062		0.01871
$f^{\downarrow}$	−3.6348	0.00263	0.00263		0.01072	0.02134
$s^{\downarrow}$	−3.6248	0.00010	0.00010	0.01072		0.02144
$f^{\downarrow}$	−3.6112	0.00010	0.00010		0.01082	0.02154
$p^{\uparrow}$	−3.5924	0.00027	0.00027	0.01089		0.02181
$p^{\downarrow}$	−3.5788	0.00028	0.00028		0.01110	0.02209
$d^{\uparrow}$	−3.5265	0.00044	0.00044	0.01143		0.02253
$d^{\downarrow}$	−3.5128	0.00045	0.00045		0.01155	0.02298
$f^{\uparrow}$	−3.4190	0.00065	0.00065	0.01208		0.02363
$f^{\downarrow}$	−3.4052	0.00067	0.00067		0.01222	0.02430
$g^{\uparrow}$	−3.3825	0.00052	0.00052	0.01260		0.02482
$g^{\downarrow}$	−3.3687	0.00052	0.00052		0.01274	0.02534
$g^{\uparrow}$	−3.1987	0.00186	0.00186	0.01446		0.02720
$g^{\downarrow}$	−3.1811	0.00188	0.00188		0.01462	0.02908
$s^{\uparrow}$	−2.4057	0.00081	0.00081	0.01527		0.02989
$s^{\downarrow}$	−2.3931	0.00083	0.00083		0.01545	0.03072
$p^{\uparrow}$	−2.3779	0.00120	0.00120	0.01647		0.03192
$p^{\downarrow}$	−2.3652	0.00124	0.00124		0.01669	0.03316
$d^{\uparrow}$	−2.3243	0.00163	0.00163	0.01810		0.03479
$d^{\downarrow}$	−2.3117	0.00177	0.00177		0.01846	0.03656
$f^{\uparrow}$	−2.2369	0.00295	0.00295	0.02105		0.03952
$f^{\downarrow}$	−2.2243	0.00307	0.00307		0.02153	0.04259
$g^{\uparrow}$	−2.1470	0.00082	0.00082	0.02188		0.04341
$g^{\downarrow}$	−2.1343	0.00066	0.00066		0.02219	0.04407
$s^{\uparrow}$	−1.7144	0.02416	0.02416	0.04601		0.06823
$s^{\downarrow}$	−1.7027	0.02466	0.02466		0.04685	0.09289
$p^{\uparrow}$	−1.6452	0.03681	0.03681	0.08285		0.12970
$p^{\downarrow}$	−1.6332	0.03741	0.03741		0.08426	0.16711
$d^{\uparrow}$	−1.5297	0.03739	0.03739	0.12024		0.20450
$d^{\downarrow}$	−1.5175	0.03742	0.03742		0.12168	0.24192
$f^{\uparrow}$	−1.3734	0.01179	0.01179	0.13203		0.25371
$f^{\downarrow}$	−1.3612	0.01190	0.01190		0.13358	0.26561
$g^{\uparrow}$	−1.1853	0.00489	0.00489	0.13692		0.27050
$g^{\downarrow}$	−1.1732	0.00492	0.00492		0.13850	0.27542
$s^{\uparrow}$	−0.9879	0.17812	0.17812	0.31504		0.45354
$s^{\downarrow}$	−0.9790	0.18037	0.18037		0.31887	0.63391
$p^{\uparrow}$	−0.8253	0.28087	0.28087	0.60491		0.92378
$p^{\downarrow}$	−0.8160	0.29418	0.29418		0.61305	1.21796
$d^{\uparrow}$	−0.7496	3.10445	3.10445	3.70936		4.32241
$d^{\downarrow}$	−0.7267	2.80486	2.80486		3.41791	7.12727
$d^{\uparrow}$	−0.5729	1.56035	1.56035	5.26971		8.68762
$d^{\downarrow}$	−0.5534	1.80220	1.81238		4.73029	10.00000
$s^{\uparrow}$	−0.4996	0.07929				
$f^{\uparrow}$	−0.4991	0.03147				
$s^{\downarrow}$	−0.4928	0.07831				
$f^{\downarrow}$	−0.4902	0.03124				
$p^{\uparrow}$	−0.4138	0.22955				
$p^{\downarrow}$	−0.4078	0.22880				
$g^{\uparrow}$	−0.3780	0.00710				
$g^{\downarrow}$	−0.3702	0.00700				
$d^{\uparrow}$	−0.1954	0.46837				
$d^{\downarrow}$	−0.1877	0.49336				
$s^{\uparrow}$	−0.1140	0.01413				
$s^{\downarrow}$	−0.1131	0.01383				

FIGURE CAPTIONS.

FIGURE 1.- Crystal potential of majority-spin for *fcc* palladium. The self-consistent procedure is carried out inside the central Wigner-Seitz cell, $0 < r < R_{WS}$, whereas the potential of the environment, $V(r > R_{WS})$, remains frozen. Number of atoms in each layer are indicated by figures under peaks.

FIGURE 2.- Radial distribution function of the highest occupied *d*-orbitals of majority-spin in *fcc* palladium, which corresponds to e_g and t_{2g} orbitals of a cubic symmetry. Arrows stands for layers positions. Central cell's Wigner-Seitz radius also is indicated.

FIGURE 3.- The same as figure 2, for *fcc* nickel.

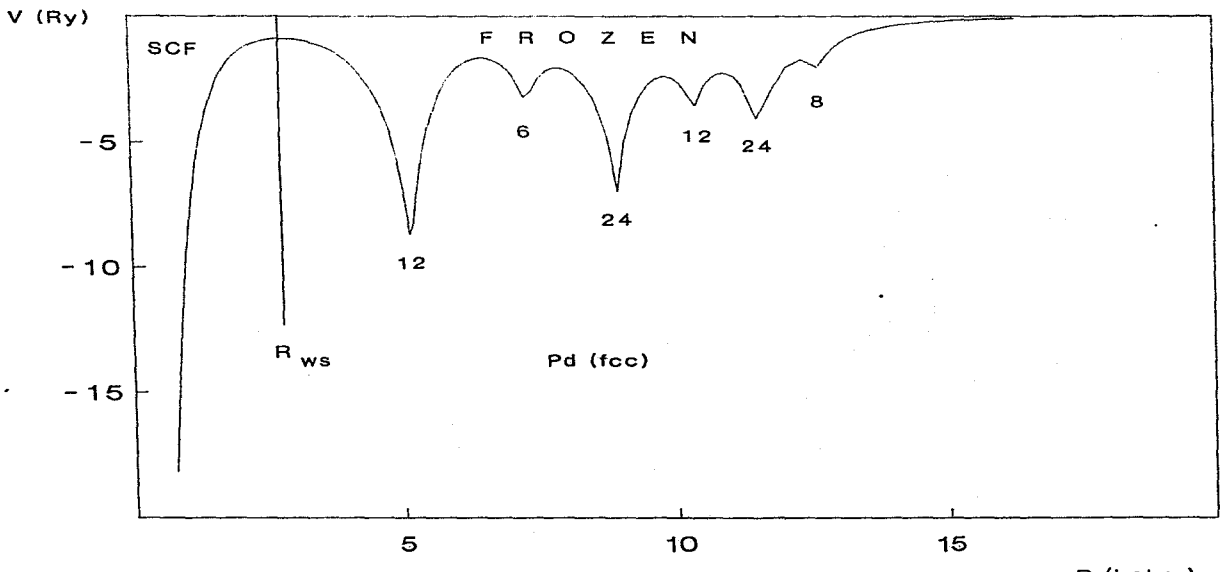
V (Ry)
SCF
F R O Z E N
-5
-10
-15
6
12
24
12
24
8
R ws
Pd (fcc)
5
10
15
R (bohrs)

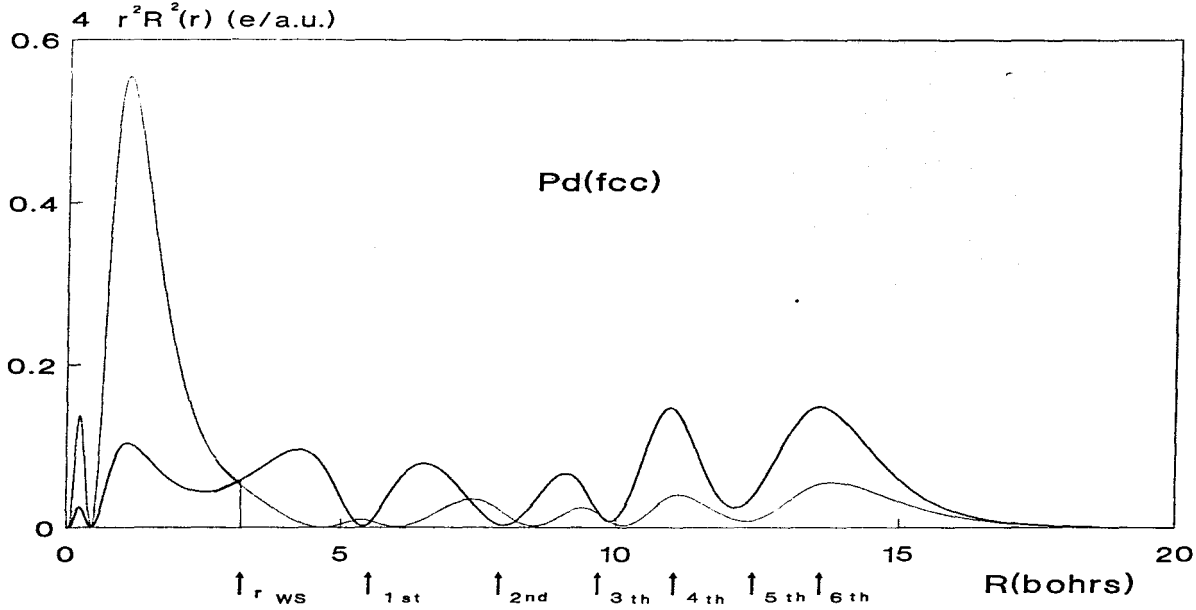
4 r²R²(r) (e/a.u.)
0.6
0.4
0.2
0
Pd(fcc)
0
5
10
15
20
R(bohrs)
r ws
1 st
2nd
3 th
4 th
5 th
6 th

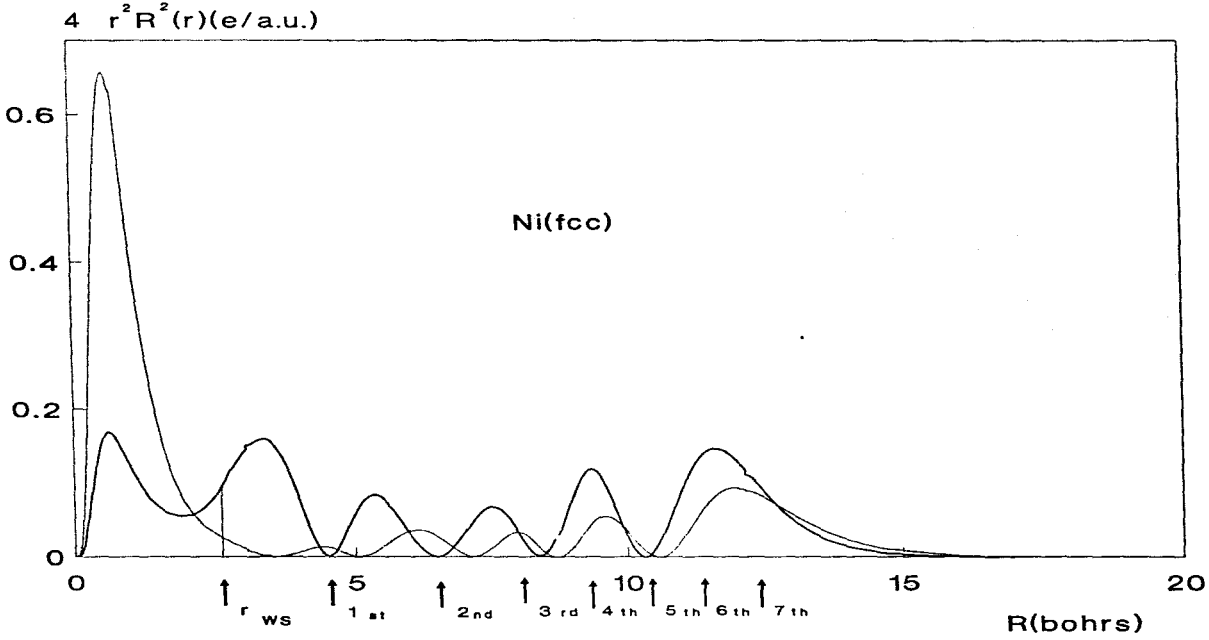
4 r²R²(r)(e/a.u.)
0.6
0.4
0.2
0
Ni(fcc)
0
5
10
15
20
r ws
1 st
2nd
3 rd
4 th
5 th
6 th
7 th
R(bohrs)

INTERACTION BETWEEN HYDROGEN AND MAGNETIC CLUSTERS. Adsorption of Atomic and Molecular Hydrogen in a Ferromagnetic Nine Atom Nickel Cluster. The Atop Case.

Miguel Castro, René Magallanes, Angeles Cuán and Vicente Soria.
Sección de Química Teórica, Facultad de Química, Universidad Nacional Autónoma de México,
Delegación Coyoacán, 04510 México D.F., México.

and

Jorge Martínez-Peniche
Departamento de Ciencias Químicas, Facultad de Estudios Superiores Cuautitlán, UNAM, Cuautitlán Izcalli 54740,
Edo. de México, México.

ABSTRACT.

We applied the multiple scattering techniques and a local spin density functional for exchange-correlation effects in order to study the adsorption of atomic and molecular hydrogen in an atop reaction coordinate over a nine atom nickel cluster. This method allows a simultaneous analysis of the competitive local effects between magnetization and chemical bond formation, that occurs during the early steps of hydrogen chemisorption. Our main results obtained from the total energy curve for the hydrogen-cluster interactions are: a binding energy of 20.97 kcal/mol at the equilibrium Ni-H distance of 2.06 Å with a vibrational frequency of 2923 cm^{-1}; at this state remains 0.182 unpaired electrons at the hydrogen site, while the cluster magnetization is reduced and changes its distribution drastically. Analysis of the SCF electronic structure shows i) a major delocalized Ni 4s-H bonding but also a significant contribution of the Ni 3d electrons, including those of the nearest neighbors to the atom involved in the bonding to the adsorbate, ii) polarization effects, from 4*p* electrons, also play an important role and iii) a small electronic charge transfer from the cluster to H occurs. On the other hand, we obtain that this reaction coordinate, in this small cluster, is unable to trap a hydrogen molecule.

INTRODUCTION.

The study of small atomic clusters is of special relevance nowadays because of its connection with the catalytic properties of fine grain materials, surface science, astrophysics and inorganic chemistry, just to mention a few of the most important fields related with this theme[1,2]. In fact, an active multidisciplinary research has evolved in order to synthesize and investigate the properties of isolated atomic clusters containing from two up to several hundred atoms of a given material[3,4,5,6]. Due to structural arrangements and to unsaturated valence effects atoms in these clusters show an strongly surface character, their physicochemical properties may well reflect some electronic structure details of the bulk surface, particularly those of local character such as chemical activity and magnetism that occurs in low dimensional transition metal systems. In the spirit of this correlation, theoretical approaches to surface reactivity usually start with calculations on a small cluster of atoms. The cluster size is inverse to the sophistication level at which are described the basic electronic interactions. In some treatments the cluster contains only one atom[7]. The adsorbate cluster interactions are then carried out and, in any case, the final results are extrapolated to those of the bulk surface.

However, the reactivity of small iron clusters with hydrogen molecules is lower and different from that of bulk surface, the experimental results show a complicated structure, with an enhanced reactivity in the 9 to 14 atoms cluster region[4,5,6], the limit surface behaviour appears abruptly for clusters containing 23 atoms or more. While for nickel all clusters are active but with a slow, steady increase of reactivity with cluster size[6]. All these results represents *per se* a challenge to any theoretical approach. An account of such results must be given in terms of the cluster electronic structure details.

On the other hand, some experimental spectroscopic techniques have been developed in order to characterize the magnetic states of metallic surfaces[2]. Now we have experimental evidence of a lot of different magnetic states in these low dimensional systems[2]. This fact has motivated the study of the effects of the adsorbates on the surfaces electronic structure properties[8]. However, an experimental characterization of hydrogen adsorbed on a surface is difficult due to the very small cross section of the hydrogen atoms and hence the help of theoretical calculations are necessary for a correct interpretation of experimental data.

It is difficult to analyze simultaneously, with the same theoretical tool, the responsible properties of a chemisorption process that involves transition metals. For instance, by means of a LAPW calculation[8] of hydrogen layers adsorbed over nickel slabs

it has been found 1.79 Å for the Ni-H equilibrium distance, corresponding to the closest center approach. But this type of calculation does not allow an analysis of the magnetic changes that occur during the primary chemisorption process steps. With a spin polarized calculation it has been found that the nickel surface magnetization is reduced to 0.2 spa[9] after hydrogen chemisorption, at the fixed Ni-H distance of 1.8 Å, but it was not reported a total energy adsorption curve with that technique.

In this paper we perform an all electron calculation, using the Multiple Scattering Cellular $X_{\alpha\beta}$ method[10], to study the competitive effects of magnetization and chemical bonding, both of a single hydrogen atom and a hydrogen molecule on an atop position over a nine atom nickel cluster. The geometry of the cluster is that of a half face-centered-cubic cell (C_{4v}): a nickel atom with its four nearest neighbors in the (100) plane and its four nearest neighbors in the (100) plane inmediately below (see figure 1).

COMPUTATIONAL PROCEDURE.

First we calculated the SCF electronic structure of a bare Ni_9 cluster in the geometry explained above. The nickel-nickel interatomic distance was initially set equal to that of bulk nickel metal. As mentioned our theoretical approach is a cellular spin polarized calculation, multiple scattering, all electron calculation by means of the $X_{\alpha\beta}$ approximation for exchange-correlation effects, with $\alpha = 2/3$ and $\beta = 0.0025$. We do

the simplification of treating inner molecular orbitals as core electrons. In previous studies the multiple scattering techniques[11,12] have given a reasonable description for the nickel ferromagnetic phase[11], the atomic hydrogen absorption in the ferromagnetic nickel bulk[12], as well as its ability to account for dissociative chemisorption at the magnetic surface of that material[11]. These calculations used the same $\alpha\beta$ parameters quoted above. In the present work, molecular boundary conditions[11] are imposed to Ni_9 , Ni_9- H and Ni_9- H_2 systems in order to gain some insight of the local magnetic order and chemical bonding capabilities in small nickel clusters.

In Ni_9 , the Ni cells radii, 1.428 Å, used in this calculation correspond to a 15 per cent enlargement with respect to the tangent sphere case and avoids an excessive overlap of the atomic Ni spheres in the highly close packed nine cluster, also avoids a prohibitive simultaneous overlap of three atomic Ni centers, see Fig. 1. In Ni_9-H, the Ni sphere radii were kept at the same value employed in Ni_9 , whereas the hydrogen cell was fixed at 1.2 bohrs. We proceeded with the calculation varying the distance of a single hydrogen atom over the central nickel atom, Ni_C, at the top of the cluster in a vertical approach, conserving all time the C_{4v} symmetry (see Fig. 1), from 1.59 Å to 3.2 Å in order to obtain the potential curve for the chemisorption state. Now, for the outer sphere we choose a radius of 4.66 Å, a size big enough to enclose all the atomic spheres and to allow the Ni_C-H internuclear distance separations. Subsequently, the same procedure was applied to molecular hydrogen. Later on the distance

between hydrogen atoms in the molecule was varied. In this approach the explicit inclusion of the 4*s*, 4p, and 3*d* valence electrons in the SCF process, at the same accuracy level (no crude assumptions are made for 3*d* electrons), allows their participation in the cluster-adsorbate chemical bond formation.

RESULTS Ni_9.

The final picture of the SCF electronic structure for the Ni_9 cluster is shown in figure 2 . Its main characteristics are typical of a ferromagnetic system: i) A completely filled majority spin-up *d*-band while the minority spin-down *d*-band is partially filled and has some unoccupied levels just above the Fermi level (E_f). In this cluster the unoccupied 3*d* band structure is essentially of minority-spin character. Our total band width for d electrons is 3.7 eV. Experimental values from 3.3 to 3.0 eV are reported for bulk nickel[13,14]. On the other hand, the SCF-LSD-SW method[15] yields a total *d*-band width of 3 eV for a Ni_{14} cluster while the ab-initio calculations obtain a value of about 6 eV for a Ni_6 cluster[16], and the X_α-SW method[17] gives a band width of 2 eV using a cluster of six atoms. ii) The bottom of both bands are of *s* character, at 5.41 eV and 5.32 eV below E_f, for the spin-up and spin-down bands, respectively; both levels correspond to the a_1 irreducible representation. This constitutes the genesis of a *s* band with a small exchange splitting of 0.09 eV. iii) However, the exchange splitting for the levels of *d*-character

depends strongly on the irreducible representation; ranging from a value of 0.24 eV for a_1, increases to 0.375 eV for e, 0.487 eV for b_1, 0.575 eV for a_2 and still it reachs a value of 0.594 eV for the b_2 irreducible representation. An exchange splitting of 0.60 eV is obtained for this kind of clusters by similar techniques[15].

The charge distribution analysis in the Ni_9 cluster shows an anisotropic magnetic distribution. The upper central atom, Ni_c, with a nearest neighbor number (NN) of 8, acquires a magnetization of 0.13 spins per atom(*spa*). The other four atoms in the upper plane, Ni_1, with a NN of 3, have a magnetization of 0.563 *spa* each. The four atoms in the plane below, Ni_2, with a NN of 5, have a magnetization of 0.415 *spa*. The entire nickel face-centered-cubic cell in free space, a Ni_{14} cluster, shows a similar magnetic distribution[15] with $Ni_c = Ni_2 = +0.435$ *spa* and $Ni_1 = +0.721$ spa, an analogous trend to that of Ni_9 but with different magnetic moment numbers, reflecting clearly the high sensibility of magnetism on cluster size and geometry. The small magnetization of the central atom in the Ni_9 cluster is due to the fact that this atom alone is bonding directly to eight nickel atoms.

Further study of the Ni_9 cluster shows that the central atom is unstable against an antiferromagnetic transition, with an energy change of $\Delta E = -0.018$ Ry if the spin of the central atom is reversed. This coupling is stronger than that found in bulk fcc nickel, $\Delta E = +0.0128$ Ry[12]. Of course, the Ni_9 cluster is unstable in the studied geometry, it can only exist if trapped in a matrix or stabilized on a surface. In any case chemical bonding effects

dominate over intraatomic exchange effects, but the intraatomic exchange is strong enough to impose an overall magnetization on the cluster. In bulk nickel our calculations yields a magnetization of 0.487 spa[11]. Defects, surfaces and small clusters of nickel must therefore show a larger magnetization per atom, with interesting ferro- and antiferromagnetic couplings.

RESULTS Ni_9-H.

In figure 3 we report the total energy dissociation curve of a single hydrogen atom approaching the nine atom nickel cluster. It can be seen that the potential surface is fairly sharp as was predicted for an atop hydrogen chemisorption site[18]. From our spin polarized SCF total energy calculations we found the Ni-H equilibrium distance at 2.06 Å. Although it is difficult to determine the position of atomic hydrogen on surfaces experimentally, LEED experimental results give 1.84 ± 0.06 Å [19] for the nickel-hydrogen bond distance whereas neutron inelastic scattering (NIS) techniques give a value of 1.88 ± 0.03 Å[20]. Both values suggest a threefold site hydrogen occupation. For H adsorption on the Ni(111) surface, ab-initio valence orbital CI calculation obtains a Ni-H bond length of 1.87 Å, 1.81 Å and 1.61 Å for a center threefold, bridge and atop sites, respectively[18], without considering magnetic effects. In the same line, a LAPW calculation[8] of hydrogen layers adsorbed over nickel slabs finds a 1.80 Å Ni-H equilibrium distance for a fourfold center approach.

In our calculations, as recognized previously[8], the explicit inclusion of magnetic effects increases the Ni-H bond length. However, in this small cluster, Ni_9, the Ni-H bond length is too large, 2.06 Å. Consistently, our theoretical binding energy is 20.97 kcal/mol for the atop cluster Ni_9- H reaction, with a high vibrational frequency of 2923 cm^{-1}. First principles spin-restricted Hartree-Fock calculations for a Ni_{20} cluster yields 36.8 kcal/mol bond energy and a vibrational frequency of 2219 cm^{-1} for a one H ligancy[21], while for a 26-atom nickel cluster model it is obtained a 44.60 kcal/mol binding energy and a vibrational frequency of 2332 cm^{-1} for the atop H adsorption[18] . The experimental binding energy of H adsorbed on Ni surface is 63.0 kcal/mol[22]. However it is recognized that the atop atom adsorption site is 19 kcal/mol higher than the most stable site occupation[18]. In order to improve the bonding capability in small nickel clusters it is necessary to increase the cluster size to 20 atoms, at least[21]. But in this last case the theoretical approaches usually involve a set of approximations such as the no-participation of the nickel 3*d* and 4*p* electrons in the chemisorptive bond[21], as it is hard to include these functions for all nickel atoms in a big cluster[23]. Partial relax of these considerations gives reasonable good hydrogen binding energies in nickel clusters[23] . By example, for the on top site case the H binding energy is 59.9 kcal/mol in a Ni_{13} cluster at CI level[23], while in Ni_{14} this property is 44.95 kcal/mol or 30.8 kcal/mol, depending if the cluster is partitioned into two or three layers, respectively[23].

Our small hydrogen binding energy, ≈ 17 kcal/mol, as corrected by the zero point motion, is a consequence of the good bind among the nickel atoms in the Ni_9 cluster. The Ni_9 magnetic moments reflect this fact (0.18 spa, 0.563 spa and 0.415 spa). Starting the SCF process with each nickel atom in the $3d^9 4s^1$ configuration, the chemical bond formation, in pure Ni_9, has reduced the 18 spins per cluster still to 4.09 spins per cluster. By the same reason, the Ni_9 cluster is not capable to trap a hydrogen molecule, nor to soften the s-s H_2 bond, when it is approached with its molecular axis perpendicular to the Ni_1 plane, above the central atom, keeping the C_{4v} symmetry. However, if the nickel atom is in a less valence-saturated environment, then it is able to do that. This was the case in the Ni_2- H_2 system, in which the same multiple scattering approach[11] was employed.

In figure 4 we show the SCF eigenvalue spectra for the Ni_9- H system at the equilibrium distance. It can be seen clearly that the minority spin-down band has been shifted to lower energies while the majority spin-up band has been destabilized. In other words, the cluster-hydrogen interactions are carried out mainly between the spin-down cluster orbitals and the s hydrogen function. Specifically and by symmetry constrains those molecular orbitals occur in the a_1 representation of the Ni_9-H C_{4v} geometry. In table 1 we show their charge distribution, resolved by spin and angular momentum component, in each atomic region. We conserve the C_{4v} symmetry in the Ni_9 - H reaction. The occupied a_1 minority spin-orbitals contribute with 0.376 electrons to the hydrogen

electronic charge, while 0.194 electrons are from the majority contribution. This numbers give a 0.570 *e* total charge at the hydrogen site with a -0.182 *spa* magnetization. At large Ni - H separations the total charge at the H site is 0.520 *e* with a net spin of -0.460 *spa*(0.490 *e* and 0.030 *e* for the minority and majority orbitals, respectively). Thus, 0.05 *e* are transfered from the cluster on atop H adsorption, see Fig. 5 . For the most stable threefold adsorption site it was obtained an 0.03 *e* transference from the *d* band to hydrogen[18].

The occupied a_1 molecular orbitals of the Ni_9- H SCF electronic structure are displayed in table 1 and indicates that bonding orbitals interactions on H adsorption are spread over the whole set of the Ni cluster *s*, *p*, d, bands. There is not a single localized hydrogen segregated cluster state[24] . Our results show a wide spread in the H pattern with weak H levels which, in the minority band, ranges from 4.8 eV to 0.51 eV, below the Fermi level. Their counterparts in the majority band are of a lesser intensity and ranges from 5.58 eV to 1.40 eV. See table 1. Nevertheless there occurs a strong H level at 2.7 eV below E_F. A bigger nickel cluster, Ni_{14}-2H, places the strong H contribution at $\simeq$ 3.5 eV[15] below E_F. For a $Ni_{20}H$ cluster this state is now at about 3.8 eV[21], while for a $Ni_{26}H$ cluster it occurs at 5.4 eV[18], both below E_F. In photoemission experiments for H on Ni(111) it has been observed a single hydrogen state at 5.8 eV below E_F[25].

The explicit inclusion of the 4*s*, 4*p*, and 3*d* valence electrons, at the same accuracy level, allows their participation in the chemical bond formation on H adsorption. The cluster interacts mainly through the 4*s* band, in an entirely delocalized mechanism, but in this case, Ni_9, there exist an important 3*d* orbital contribution. The level at 3.45 eV below E_F contains one of the 3*d*-H contributions with 0.65 *d* and 0.04 H populations. The strong H resonance, at 2.7 eV, also contains a significant *d*-H mixing with 0.25 *d* and 0.15 *d* electrons per atom in the sublayer (Ni_2) and first layer (Ni_1), respectively, while the central nickel atom has 0.04 4*s* and 0.04 4*p* electrons in this level. In other words, all nearest neighbors of the atom involved in the bonding to the adsorbate, also are included in the bond. A similar behaviour has been observed in beryllium[26] and nickel[23] clusters, where a better description is obtained when the 4*p* function is included in the chemisorption region[23]. In our case, polarization effects from 4*p* electrons, also play an important role. This last can be appreciated in table 3 where is reported a charge distribution analysis[27] and magnetizations of the nickel (4*s*, 3d, and 4*p*) and hydrogen (1*s*) valence electrons at the Ni_9- H total energy minimum state. In closer detail, the total charge distribution analysis per spin and per angular moment component, in each atomic region, is presented in table 2. The charge in the outer and interstitial regions was assigned to the atoms by means of two different charge distribution schemes[27,28] . The final atomic populations, in both approaches, shows a similar trend. We report those obtained with the method of reference 27.

The average magnetization in pure Ni_9 is of 0.454 *spa* while in Ni_9- H that average is of -0.085 *spa* ignoring H. Including it the number is -0.100 *spa*. See table 3. The cluster magnetization has dead on H chemisorption.

In order to chemisorb a single hydrogen atom the small nickel cluster has moved his electronic cloud to the region where the chemical reaction takes place, putting enough unpaired electrons for the process at that site. From the sublayer, Ni_2, flows ≈ 0.4 electrons to the top layer, Ni_1 + Ni_c, which produces an excess of charge and an increase of the magnetization, instead of a decrease, at the central nickel atom. See table 3. Locally, the cluster-adsorbate chemical bond formation may be viewed as the usual paired electrons process: $Ni_c^{0.60\uparrow}$ - $H^{0.24\downarrow}$.

CONCLUSIONS.

The multiple-scattering techniques combined with LSD functionals for the construction of exchange-correlation potentials are able to account for basic electronic interactions in transition metal clusters, and small transition metal clusters-adsorbates, in free space. The SCF-electronic structure allows an analysis of the interplay between magnetic couplings and

chemical bonding effects that occurs in such systems. In both cases chemical bonding dominate over intraatomic exchange effects, but this interaction is strong enough to impose an overall magnetic order on small clusters, which shows a high magnetization per atom, with interesting ferro- and antiferromagnetic couplings.

The inclusion of all valence electrons (4*s*, 3*d*, and 4*p*) results in a good bind for the cluster and in consequence a low binding energy for the cluster-adborbate chemical reaction, but those functions have moved the cluster electronic charge in such a way to promote that process. At the end, the H chemisorption have canceled almost entirely the cluster magnetization, but the local magnetic structure, as well as the nature of the cluster-adsorbate chemical bond, are quite different from those that occurs in an extended nickel surface during hydrogen chemisorption. Small clusters not necessarily reflect all the electronic structure details of the entire surface and they are more demanding with respect to the input basis set for a better description of their properties.

ACKNOWLEDGEMENTS.

It is a pleasure to acknowledge to all the staff of the Programa Universitario de Computo - UNAM.

REFERENCES.

1.- Computational Chemistry: The Challenge of *d* and *f* electrons; D.R. Salahub; M.C. Zerner, Eds.; ACS Symposium Series No. 394; American Chemical Society; Washington, DC, 1989.

2.- Magnetic Properties of Low-Dimensional Systems; Falicov, L.M. and J.L. Morán-López , Eds.; Springer-Verlag; Neetherlands 1986.

3.- W. L. Brown, R. R. Freeman, Krishnan Raghavachari, and M. Schluter, Science 235, 860 (1987).

4.- R. L. Whetten, D. M. Cox, D. J. Trevor, and A. Kaldor, Phys. Rev. Lett. 54, 1494 (1985), and references therein.

5.- S. C. Richtsmeier, E. K. Parks, K. Liu, L. G. Pobo, and S. J. Riley, J. Chem. Phys. 82, 3659 (1985).

6.- M.D. Morse, M.E. Geusic, J.R. Heath and R.E. Smalley, J. Chem. Phys. 83, 2293 (1985).

7.- J. Garcia-Prieto, M. E. Ruiz, and O. Novaro, J. Am. Chem. Soc., 107, 5635 (1985).

8.- C. Umrigar and J.W. Wilkins , Phys Rev. Lett. 54, 1551 (1985).

9.- M. Weinert and J. W. Davenport , Phys. Rev. Lett. 54,, 1547 (1985).

10.- (a) A. Garritz, J. L. Gázquez, M. Castro and J. Keller, Int. J. Quantum Chem. 15, 731 (1979).

(b) M. Castro, J. Keller and P. Rius, Hyperfine Interactions 12, 21 (1982).

(c) M. Castro, J. Keller and O.N. Ventura, J. Chem. Phys. 77, 6348 (1982).

11.- J. Keller, M. Castro, and A.L. de Paoli, J. Appl. Phys. 53, 8850 (1982).

12.- J. Keller and M. Castro, J. Magn. Magn. Mater. 15-18, 856 (1980).

13.- D. E. Eastman and J. K. Cashion, Phys. Rev. Lett. 27, 1520 (1971).

14.- S. Hufner, G.K. Wertheim, N.V. Smith and M.M. Traum, Solid State Commun. 11, 329 (1972).

15.- R. Fournier and D. R. Salahub, Int. J. of Quantum Chem., XXIX, 1077 (1986).

16.- H. Basch, M.D. Newton and J.W. Moskowitz, J. Chem. Phys. 73, 4492 (1980).

17.- N. Rosch and D. Menzel, Chem. Phys. 13, 243 (1976).

18.- H. Yang and J.L. Whitten , J. Chem. Phys. 89, 5329 (1988).

19.- K. Christmann, R. J. Behm , G. Ertl , M. A. Van Hove and W. H. Weinberg , J. Chem. Phys. 70, 4168 (1979).

20.- R. R. Cavanagh , R. D. Kelley and J.J. Rush, J. Chem. Phys. 77, 1540 (1982).

21.- H. T. Upton and W. A. Goddard III, Phys. Rev. Lett. 42, 72 (1979).

22.- K. Christmann, O. Schober, G. Ertl, and M. Newmann, J. Chem. Phys. 60, 4528 (1974).

23.- P. E. M. Siegbahn, M. R. A. Blomberg and C. W. Bauschlicher, J. Chem. Phys. 81, 2103 (1984).

24.- F. J. Himpsel, J. A. Knap, and D. E. Eastman, Phys. Rev. B 19, 2872 (1979).

25.- J. E. Demuth, Surf. Sci. 65, 369 (1977).

26.- C. W. Bauschlicher, P. S. Bagus, and H. F. Schaefer, IBM J. Res. Develop. 22, 213 (1978).

27.- A. Garritz and A. Vela, Chem. Phys. Lett. 73, 84 (1980).

28.- D. A. Case and M. Karplus, Chem. Phys. Lett. 39, 33 (1976).

Table 1.- Electronic charge distribution of the occupied a_1 molecular orbitals at the Ni_9- H total energy minimum. The charge, in electrons, in sub- and first layers is for 4 Ni atoms. The zero monoelectronic energy corresponds to the Fermi level.

ε_i(eV)	spin	Ni_c-central			Ni_1-first layer			Ni_2-sublayer			Hydrogen
		s	*p*	*d*	*s*	*p*	*d*	*s*	*p*	*d*	*s*
5.58	↑	0.281	0.023	0.000	0.116	0.056	0.040	0.276	0.096	0.052	0.005
3.74	↑	0.002	0.002	0.752	0.024	0.012	0.028	0.008	0.020	0.128	0.011
2.49	↑	0.045	0.008	0.004	0.004	0.024	0.160	0.136	0.004	0.492	0.030
2.12	↑	0.008	0.062	0.069	0.028	0.000	0.024	0.012	0.020	0.508	0.096
1.85	↑	0.000	0.014	0.003	0.016	0.000	0.088	0.016	0.000	0.752	0.014
1.40	↑	0.008	0.019	0.055	0.000	0.000	0.288	0.016	0.000	0.484	0.038
0.53	↑	0.000	0.000	0.006	0.020	0.000	0.752	0.000	0.016	0.140	0.000
0.03	↑	0.002	0.000	0.016	0.000	0.000	0.764	0.008	0.000	0.172	0.000
4.80	↓	0.281	0.020	0.000	0.120	0.052	0.044	0.276	0.096	0.060	0.012
3.45	↓	0.001	0.000	0.651	0.028	0.012	0.036	0.000	0.016	0.180	0.039
2.70	↓	0.038	0.045	0.000	0.000	0.024	0.148	0.140	0.012	0.248	0.146
2.41	↓	0.000	0.041	0.011	0.028	0.000	0.080	0.000	0.008	0.620	0.086
2.00	↓	0.000	0.003	0.023	0.012	0.000	0.080	0.028	0.000	0.776	0.002
1.58	↓	0.003	0.006	0.124	0.008	0.000	0.300	0.008	0.000	0.504	0.013
0.82	↓	0.000	0.000	0.008	0.016	0.000	0.756	0.000	0.012	0.160	0.000
0.67	↓	0.000	0.001	0.007	0.004	0.000	0.768	0.008	0.000	0.160	0.008
0.51	↓	0.001	0.002	0.120	0.000	0.008	0.584	0.008	0.004	0.096	0.072

Table 2.- Total charge distribution analysis per spin and per angular momentum component, in each atomic region of the Ni_9-H system at the total energy minimum. The charge is in electrons.

Atom	Spin	s	p	d
Hydrogen	↑	0.25375	0.00226	0.00000
	↓	0.48958	0.00204	0.00000
	↑ + ↓	0.74333	0.00430	0.00000
	↑ − ↓	-0.23583	0.00022	0.00000
Ni_c (central)	↑	3.36603	6.52681	4.62706
	↓	3.24214	6.44572	4.12768
	↑ + ↓	6.70817	12.97253	8.75474
	↑ − ↓	0.02389	0.08109	0.49938
Ni_1 (first layer)	↑	3.44733	6.11990	4.33758
	↓	3.39617	6.11649	4.63957
	↑ + ↓	6.84350	12.23639	8.97715
	↑ − ↓	0.05116	0.00341	-0.30199
Ni_2 (sublayer)	↑	3.34147	6.19214	4.36759
	↓	3.30420	6.16936	4.52242
	↑ + ↓	6.64567	12.36150	8.89001
	↑ − ↓	0.03727	0.02278	-0.15483

Table 3.- Charge distribution and magnetizations of nickel (4*s*, 3*d*, and 4*p*) and hydrogen (1*s*) valence electrons at the Ni_9 - H total energy minimum.

Atom	Electronic Configuration (*per atom*)			Magnetization (*spa*)*	Total valence electrons**
H		$1s^{0.743}$		-0.236	0.743
Ni_c	$4s^{0.708}$	$3d^{8.754}$	$4p^{0.973}$	+0.604 (0.180)	10.435 (10.232)
Ni_1	$4s^{0.844}$	$3d^{8.930}$	$4p^{0.236}$	-0.247 (0.563)	10.060 (9.936)
Ni_2	$4s^{0.646}$	$3d^{8.890}$	$4p^{0.362}$	-0.095 (0.415)	9.898 (10.006)

* spins per atom, values in parentheses are for the Ni_9 cluster.

** Values in parentheses are for the Ni_9 cluster.

FIGURE CAPTIONS

Fig. 1 Geometry structure and space partitioning for Ni_9- H. Labels within circles are for the atomic regions: H - hydrogen, C - central nickel atom, 1 - nickel first layer, and 2 - nickel sublayer. The Ni_9 cluster is without considering the H region.

Fig. 2 Molecular orbital eigenvalues for the Ni_9 cluster: ($\uparrow$) - majority spin, ($\downarrow$) minority spin. The dashed line indicates the position of the Fermi level (E_f).

Fig. 3 Total energy (in Ry) of the Ni_9- H system as a function of the Ni_C- H internuclear distance (in Å).

Fig. 4 Molecular orbital eigenvalues for Ni_9- H: ($\uparrow$) - majority spin, ($\downarrow$) minority spin. The dashed line indicates the position of the Fermi level (E_f).

Fig. 5 Behaviour of the charge (in electrons) inside hydrogen region, in Ni_9- H, as a function of the Ni_C- H internuclear distance (in Å).

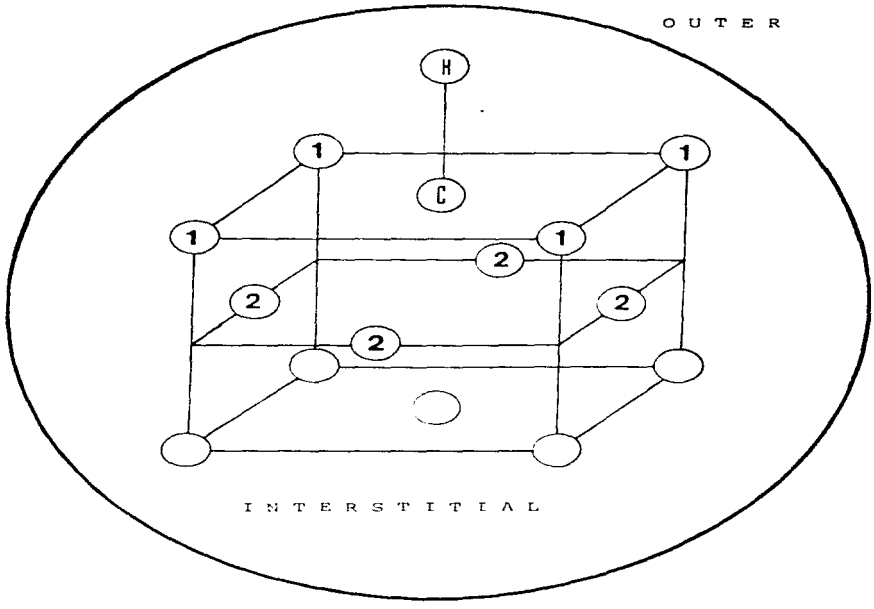

Figure - 1

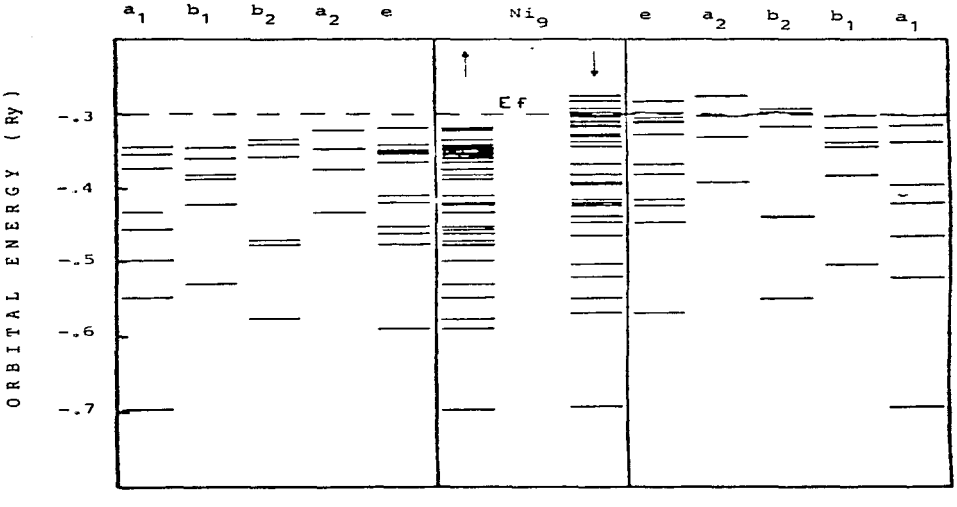

Figure - 2

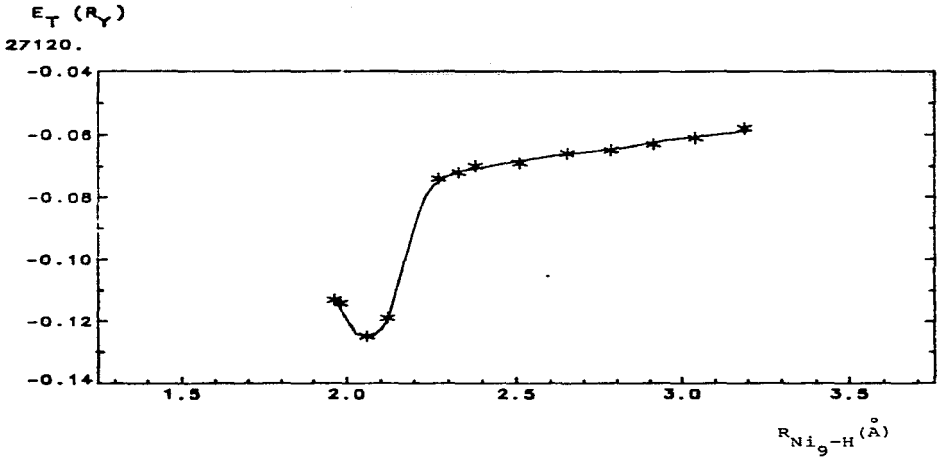

Figure - 3

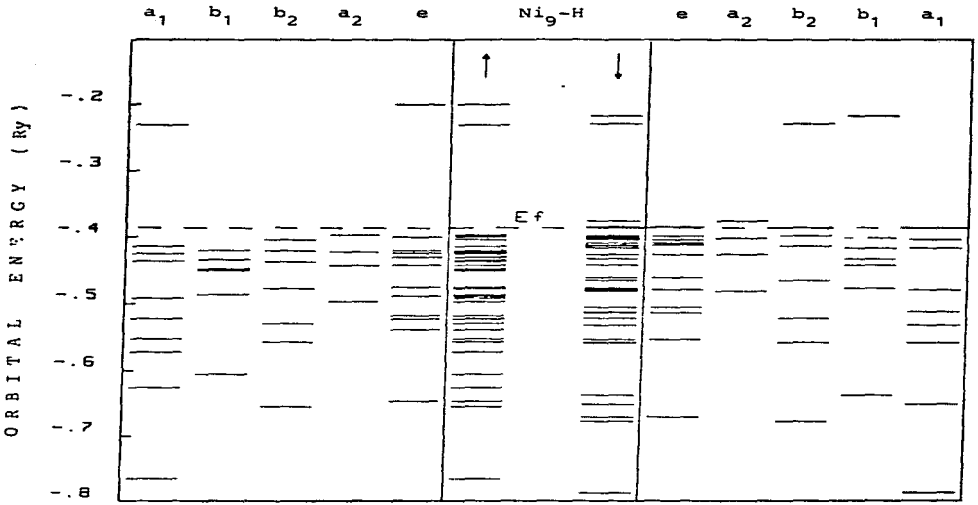

Figure - 4

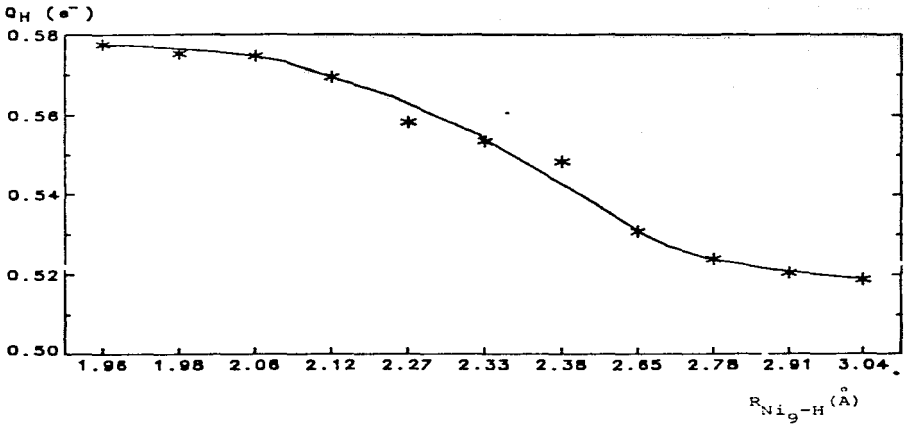
Q_H (e^-)
0.58
0.56
0.54
0.52
0.50
1.96
1.98
2.06
2.12
2.27
2.33
2.38
2.65
2.78
2.91
3.04
R_{Ni_9-H} (Å)

Figure - 5

Hyperfine Interactions 12(1982)261–278 261

ISOTOPE EFFECT IN CHEMICAL SHIFTS OF μ^+ AND H^+: MuBr versus HBr and MuHO versus H_2O

M. CASTRO*, J. KELLER* and P. RIUS

Facultad de Química, Universidad Nacional Autónoma de México, Apartado Postal, 70-213 Coyoacán, D.F. - México

and

Institute for Theoretical Physics, Eidgenössische Technische Hochschule, CH-8049 Zurich, Switzerland

Received 12 February 1982
(Revised 8 June 1982)

The isotopic difference between the diamagnetic shielding of a positive muon (μ^+) in μ^+-substituted HBr and H_2O and the analogous shielding of protons is computed from first principles in free space and in CF_4 solution, using a self-consistent cellular cluster multiple scattering method (SC-CMS) for condensed matter and for the free molecules. The isotope shift of the chemical shift σ_{iso} at the μ^+ in these molecules dissolved in liquid HF_2 is evaluated with the eigenfunctions and eigenvalues obtained using Ransey's formalism. For HBr the computed chemical shifts σ_{iso} are comparable with experiment and with the calculations of Berkowman and Kometsky and of Williams, and the isotope effect has the correct sign and order of magnitude. For H_2O, σ_{iso} has the correct sign and order of magnitude when compared with μ^+SR experiments.

1. Introduction

The purpose of the present study is twofold: (a) to analyze the isotope and solvent chemical shifts for MuBr and MuHO molecules; and (b) to demonstrate the application of condensed matter techniques to molecular problems.

We chose HBr and H_2O because experimental measurements of μ^+ precession in MuBr and MuHO in liquid Freons are used for a high accuracy determination of the μ^+ intrinsic magnetic moment [1]. These measurements use muon spin rotation techniques (μ^+SR), in which positive muons are stopped in a liquid target in an externally applied magnetic field, and their former frequency observed via the asymmetric decay of the muon. This method requires a precise knowledge of the effective field seen by the μ^+. This field differs from the external one because of screening effects in the chemical compound containing the muons. In the early experiments [2], water was usually used as the stopping target. However, this system will not allow an unambiguous assignment of the chemical environment and consequently limited the precision of the diamagnetic shielding corrections. In order to avoid this problem, in recent experiments pure bromine was employed as the liquid target. In this case only one molecular species containing the muon is formed:

$$Mu + Br_2 \rightarrow MuBr + Br \,. \qquad (1)$$

However, a small water contamination of the bromine produces the MuBr dissociation

$$MuBr + H_2O \rightarrow (MuH_2O)^+ + Br^- \quad (2)$$

and proton exchange takes place,

$$(MuH_2O)^+ + H_2O \rightarrow MuD + (H_3O)^+ \quad (3)$$

For both the dry and the wet Br_2 sample, the μ^+SR frequency has been determined to a high precision. It was found that the liquid association shift for MBr and H_2O are -1.92 ppm and -1.18 ppm, respectively [3]. With these results, and with the assumption that the isotopic effect for both molecules is -0.50 ppm, a very exact value for the muon's magnetic moment was obtained by this experimental technique. One of the main purposes of this work is to check these assumptions by means of a first principles calculation using multiple scattering techniques.

2. Computational method and procedures

The calculation was carried out with a cellular multiple scattering technique (Keller, 1973, 1975) [4] using electron gas theory statistical exchange and correlation to construct total one-electron potentials [5], as described below. The condensed matter boundary conditions are introduced as in Keller 1971, 1972 [6]. The calculation is from first principles except for the simplifications made in the analysis of the μ^+ chemical shielding.

The method used is suitable for the computation of the electronic properties of molecules and of clusters of atoms embedded in a material. The material may be solid (crystalline or glassy) or fluid. The embedding medium is represented by its effect on the electrons through a potential which represents, at least in an approximate way, the appropriate boundary conditions for electron waves in condensed matter. In general, the calculation of spin densities, charge transfers, localized or impurity states and local bonding in condensed matter is possible with full charge approaches. Properties depending on long range order in crystalline materials cannot, without modifications, be treated by the cluster method.

We should consider two types of systems: the first we will call open system, where the effect of the environment outside the cluster border is represented by an appropriate average (spherical average, for example) of its potential; the second we will call closed system, where the environment outside the cluster is represented by periodic boundary conditions or approximated, as in our case, by a finite number of atomic shells surrounding the central cluster, the potential being spherically averaged and the calculation for the central cluster carried out as for a modified molecule.

The cluster is partitioned into a collection of non-overlapping cells and an interstitial region (the region left between the cells and inside the outer sphere) where the potential is taken to be constant and equal to the volume average for this region (this will be illustrated later in fig.5).

In all these calculations, the one-electron model is used in which all interactions between electrons, except those from their coulomb repulsion, can be treated in the form of an effective potential felt by every one of the electrons through the material. The calculations of the total energy and of the charge densities are described in appendixes A and B. A simple and intuitive way to write down the

multiple scattering equations which provide solutions for the pseudo-Schrödinger equation within the Kohn-Sham theory [6] is the following: by numerical integration one finds a set of wave functions $R_L^i(\vec{r}_i,E)$, solutions of the Schrödinger equation for angular momentum L within cell i immersed in the interstitial potential V_{int}. $\vec{R}_i$ corresponds to the center of the i^{th} cell, $\vec{r}_i = \vec{r} - \vec{R}_i$, E is the pseudo-energy of the Kohn-Sham theory and $L = l,m$ stands for a couple of angular momenta quantum numbers.

Within the interstitial region, the wave functions should be constructed from a linear combination of spherical Bessel and Newman functions, these being a complete basis set for the solutions of the Schrödinger equation where a constant potential V_{int} is considered. Then, using continuity of the wave function and of its first derivative, we should obtain

$$R_L^i(\vec{r}_i,E) = j_L(k\vec{r}_i) - \sum_{L'} \kappa_{LL'}^i n_{L'}(k\vec{r}_i) \quad , \tag{4}$$

for a continuation of the wave function within the interstitial region. The matrix $\kappa_{LL'}^i$ is called the reaction matrix for cell i and the notation

$$j_L(k\vec{r}_i) = j_L(kr_i)Y_L(\hat{r}_i) \quad ,$$

$$n_L(k\vec{r}_i) = n_L(kr_i)Y_L(\hat{r}_i) \tag{5}$$

has been used. k is the magnitude of the wave vector within the interstitial region,

$$k = \sqrt{(2m/\hbar^2)(E - V_{int})} \quad ,$$

$j_L(x)$ and $n_L(x)$ are the standard Bessel and Newman functions and the $Y_L(\hat{r})$ are the real spherical harmonics.

Here we consider that the functions $R_L^i(\vec{r}_i,E)$ are solutions of the Schrödinger equation inside cell i and in the interstitial region, but not inside a cell $j \neq i$. Then the total wave function

$$\psi(\vec{r},E) = \sum_{i,L} c_{iL} R_L^i(\vec{r}_i,E) + \sum_L c_{jL} j_L(k\vec{r}) \tag{6}$$

will be a solution if the tails of all the functions $R_L^j(\vec{r}_j,E)$, $j \neq i$ cancel the contribution of the free wave, corresponding to the second term in (6), inside cell i and, moreover, if $\psi(\vec{r},E)$ satisfies continuity conditions at the inner border of the outer region.

The above conditions are found by using the translation properties of the spherical Bessel functions

$$j_L(k\vec{r}_i) = \sum_{L_1} J_{LL_1}^{ij} j_{L_1}(k\vec{r}_j) \quad , \tag{7}$$

$$n_L(k\vec{r}_i) = \begin{cases} \sum_{L_1} J_{LL_1}^{ij} n_{L_1}(k\vec{r}_j), & |\vec{r}_j| > |\vec{R}_j - \vec{R}_i| \\ \sum_{L_1} N_{LL_1}^{ij} j_{L_1}(k\vec{r}_j), & |\vec{r}_j| < |\vec{R}_j - \vec{R}_i| \end{cases} ; \tag{8}$$

here the $\mathcal{J}^{ij}_{LL'}$ and $N^{ij}_{LL'}$ are called free electron propagators and have the following properties:

$$\mathcal{J}^{ij}_{LL'} = \sum_{L''} \mathcal{J}^{ik}_{LL''} \mathcal{J}^{kj}_{L''L'} \quad , \tag{9}$$

implying

$$\mathcal{J}^{ii}_{LL'} = \delta_{LL'}$$

and are defined as follows:

$$\mathcal{J}_{L'L}(\vec{R}) = \begin{cases} k \sum_{L''} C^{L''}_{L'L} 4\pi i^{\ell_{L''}} n_{\ell_{L''}}(kr) Y_{L''}(\hat{R}) \quad , & |\vec{R}| \neq 0 \\ 0 \quad , & |\vec{R}| = 0 \quad , \end{cases} \tag{10}$$

$$N_{L'L}(\vec{R}) = \begin{cases} \sum_{L''} C^{L''}_{L'L} 4\pi i^{\ell_{L''}} j_{\ell_{L''}}(kr) Y_{L''}(\hat{R}) \quad , & |\vec{R}| \neq 0 \\ \delta_{L'L} \quad , & |\vec{R}| = 0 \quad . \end{cases} \tag{11}$$

The super indices (ij) have been replaced by $\vec{R} = \vec{R}_j - \vec{R}_i$ as an argument.

The cancellation of tails implies

$$\sum_L \left[\sum_{i \neq j} C_{iL} \left(\mathcal{J}^{ij}_{LL'} - \sum_{L''} \mathcal{J}^{i1}_{LL''} N^{1j}_{L''L'} \right) + D_L \mathcal{J}^{0j}_{LL'} \right] = 0 \quad , \tag{12}$$

using the fact that $|\vec{R}| < |\vec{r}_j|$ for $\vec{r}$ within cell j. This will restrict the sizes and shapes of the cells that can be used in practice.

The difference between open and closed systems lies in the way we impose the boundary conditions at the inner border of the outer region. As we will only use closed systems, we will restrict ourselves to this case.

At the inner boundary of the outer region, the wave function (6) is

$$\psi(\vec{r},E) \rightarrow \sum_{i,L,L'} \left(C_{iL} \mathcal{J}^{i0}_{LL'} + D_{L'} \right) j_{\ell_{L'}}(k\vec{r}) - C_{iL} \mathcal{J}^{i0}_{LL'} n_{\ell_{L'}}(k\vec{r}) \quad , \tag{13}$$

This wave function should match the inward integrated wave function $R^o_L(r)$ for the outer region. Here we should consider two different types of closed systems:

(a) Finite systems

$$\lim_{r \to \infty} R^o_L(r) \rightarrow 0 \quad ,$$

or

(b) Wigner-Seitz periodic boundary conditions

$$\left. \frac{dR^o_L}{dr} \right|_{r = R_b} = 0 \quad ,$$

where R_b is an equivalent Wigner-Seitz radius of a spherical cell appropriate for the cluster inside. When, as in the present calculation, the electronic potential in the outer cell is spherically symmetric, the $R^o_L(r)$ can be chosen to be symmetrized eigenfunctions of angular momentum L.

This wave function R^o_L can be continued in the inner border of the outer cell with the form

$$R^o_L(\vec{r},E) = -\kappa^o_{LL}\, j_L(k\vec{r}) + n_L(k\vec{r}) \quad ; \tag{14}$$

here κ^o_L is the reaction matrix of the outer sphere, assumed to be diagonal. Finally

$$\psi(\vec{r},E) = \sum_L c_{oL} R^o_L(\vec{r},E) \quad , \tag{15}$$

and the continuity at the inner border of the outer sphere implies

$$\sum_{L'}\sum_{i} c_{iL'} J^{io}_{L'L} + D_L = -\, c_{oL}\, \kappa^o_{LL} \quad ,$$

$$\sum_{L',L''}\sum_{i} c_{iL'} K^{ij}_{L'L''} J^{jo}_{L''L} = -\, c_{oL} \quad . \tag{16}$$

The coefficient D_L can now be eliminated to obtain the secular equation:

$$\sum_{\substack{i\neq j \\ L'L''}} c_{iL'} K^{ij}_{L'L''} + \sum_{L'} c_{iL'} J^{ij}_{L'L} = 0 \quad , \tag{17}$$

with the extended definition

$$K^{io}_{LL'} = J^{io}_{LL'} \qquad \text{and} \qquad K^{oj}_{LL'} = J^{oj}_{LL'} \quad . \tag{18}$$

In the present work we solve the system (17) numerically to obtain the eigenvalues E and the coefficients C_{iL} to normalize the wave function, finding states for the complete closed system cluster plus external boundary.

Back to the actual calculation, the initial step is a calculation of occupied state eigenvalues, charge densities and the HBr and H_2O molecules' internuclear distance potential energy curve shown in figs. 1a and 2a.

The calculation starts with the overlapping of atomic charge densities of atoms A and B. The sphere radii $R_A(R_B)$ which can contain $Z_A(Z_B)$ electrons around atom A(B) give a cellular ratio R_A/R_B which is kept constant during the calculation. The outer cell has in every case a muffin-tin radius. The cellular radii R_A and R_B are optimized for some set of trial bond lengths to minimize the effect of the interstitial charge (figs.3 and 4), under the constraint $(R_A/R_B) = (R^o_A/R^o_B)$ [7].

Finally, the NaBr and H_2O molecules were analyzed in a boundary potential simulating a shell of Br_2 neighbours, as shown in fig.5. The boundary potential is constructed as the one-electron potential which is obtained by smearing out a solvation layer of Br_2 molecules around the central molecule. The liquid is assumed to be closely

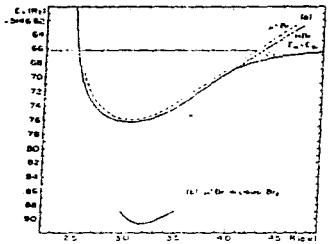

Fig.1. (a) Computed total energy of the HBr molecule as a function of the internuclear distance R. The dotted line shows the energy corrected for the finite mass of H^+. The horizontal line shows the free atom limit and the line marked C.I. the behaviour of the total energy if configuration interaction had been included. (b) Computed total energy for the molecule in the model solvent boundary conditions.

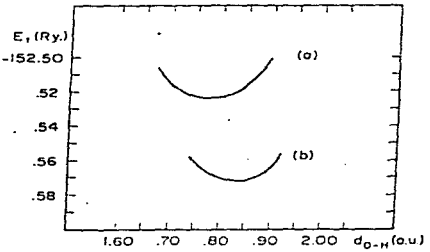

Fig.2. (a) Computed total energy of the H_2O molecule as a function of the internuclear distance R. (b) Computed total energy for the molecule in the model solvent boundary conditions.

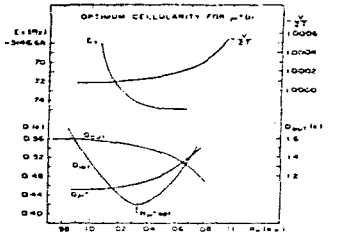

Fig.3. Behaviour of the total energy, virial ratio and charge distributions at the equilibrium HBr distance as a function of the cells' radii R_H. The optimum cellularity is taken to be that for which Q_{INT} shows a minimum value.

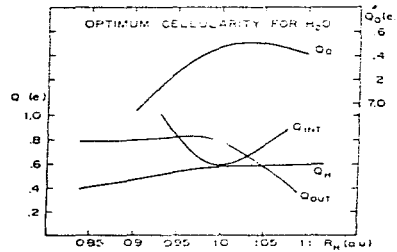

Fig.4. Behaviour of the charge distributions at the equilibrium H_2O distance as a function of the cells' radii R_H. The optimum cellularity is taken to be that for which Q_{INT} shows a minimum value. Near this point, quantities like E_T, $-V/2T$ have stable values relative to small changes in the cell radii.

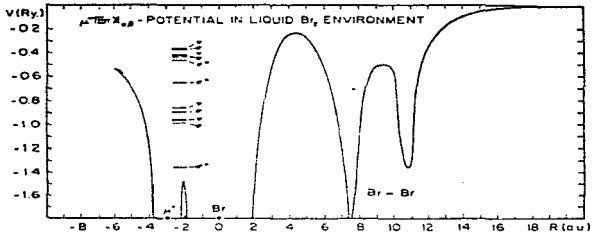

Fig.5. Molecular and boundary potentials for the MuBr molecule inside a liquid Br_2-like layer of atoms. Only the spherically symmetric part of the boundary potential is kept (unchanged) during the calculational procedure. The peak at 7.5 a.u. arises from the nearest Br atoms. The original valence states are split as shown. The ones marked * have the largest occupation and are in close correspondence with those of the free molecule.

packed, with a local density equal to the average density of liquid bromine.

The variations of the total energy with changes in the internuclear distance for the central molecules (MuBr and MuOH in Br_2-like environment) are shown in fies. 5b and 6a.

The final values of the more relevant parameters computed for free and dissolved HBr molecules are shown in table 1, where the internuclear potential energy for the study of the vibrational states is taken to be

$$V(R) = V_0(R_e) + f(R-R_e)^2 + g(R-R_e)^3 ,$$

as f and g will be used to find the expectation value

$$\overline{(R-R_e)} = (\tfrac{1}{4}\sqrt{\pi})\, g\mu^{-\frac{1}{2}} f^{-\frac{3}{2}} ,$$

for an anharmonic oscillator [8,9].

3. Isotope effect on the chemical shielding

Following Breskman and Kanofsky (BK) [8], we can compute directly the isotope shift of the chemical shielding ($\Delta\sigma_{isotope} = \sigma_{iS}$)

$$\Delta\sigma_{isotope} = \left[\overline{(R-R_e)}_{MuBr} - \overline{(R-R_e)}_{HBr} \right] \sigma' + \ldots ,$$

using the parameter $\sigma' = -13.0$ ppm/a.u. from (BK), to obtain $\Delta\sigma_{isotope} = -0.6358$ ppm. The value computed by (BK) and Williams was -0.707 ppm.

Table 1
Molecular HBr

	HBr exp.	Free HBr calc.	HBr in Br_2 calc.
Equilibrium distance R_e (a.u.)	2.67	3.053	3.190
E_{min}(Ry) at R_e		- 5146.7650	- 5146.9045
E free atom limit (Ry)		- 5146.6623	
$\Delta E_{binding}$ (Ry)		0.1047	
$\Delta E_{binding}$ (Kcal/mol) = $\frac{1}{2}\hbar\omega_e$	86.092	33.900	
f(Ry/(a.u.)^2)		0.1716	0.36
q(Ry/(a.u.)^3)		0.1000	
Vibrational frequency ω_e(cm^{-1})	2649.401	2126.160	8330.6
$E_{ZP} = \frac{1}{2}\hbar\omega_e$ (Ry)		0.0097	
$(R - R_e)$(a.u.) for HBr		0.02490	
$(R - R_e)$(a.u.) for MuBr		0.07381	
Reduced mass μ for HBr	906.702		
Reduced mass μ for MuBr	103.239		
Vibrational frequency ω_e(cm^{-1}) MuBr		6289.45	
$E_{ZP} = \frac{1}{2}\hbar\omega_e$ (Ry) for MuBr		0.02869	
$(R - R_e)_{HBr} - (R - R_e)_{MuBr}$(a.u.)		0.04691	
$\sigma' = \delta\sigma/\delta R_{HBr}$(ppm/a.u.)		- 8.05	

In our direct calculation following Ramsey's formalism [10], $\sigma' = -8.05$ ppm/a.u., a lower value. But it should be considered that our computed equilibrium bond length is too large and that σ' is given by

$$\sigma' = \sum_{(e_i)} \frac{\delta\sigma}{\delta e_i}\frac{de_i}{dR}\bigg|_{R=R_e} + \frac{\delta\sigma}{\delta R}\bigg|_{R=Re}$$

and in this expression the second term is dominant, these facts being the origin of our underestimation of σ'. The bond length R enters explicitly in χ^{Lamb} only, and can also be made to enter explicitly in a (simplified) analysis of the paramagnetic shielding [10,11] where

$$\frac{\delta\chi^{Lamb}}{\delta R}\bigg|_{R=Re} = \text{const}\ \frac{1}{(R_e)^3}$$

from which we have underestimated σ' by a factor which can be approximated from R_e(calc.)/R_e(exp.) = 1.14. Correcting this we obtain $\sigma'_{corrected}(= 1.14\,\sigma') = -13.60$ ppm/a.u. which should be a better value.

In a second step, the calculation was repeated using the heuristic approximation that in the muon cell the Schrödinger equation was solved with the $e^- - \mu^+$ reduced mass. The result is shown in fig.1b. (For an isolated muonic atom, using the same approximation and a cellular partitioning of the space, the total energy converges rapidly to the analytic value, in a test calculation increasing the radius of the muon cell.) The new parameters are $E_{min} = -5146.7005$, $R_e = 3.0549$ a.u., $f = 0.1767$ Ry/(a.u.)^2, ω_e(MuBr) = 6394.721 cm^{-1}, then, with this new calculation $\sigma' = -13.0$ ppm/a.u. and the isotope effect on the chemical shielding $\Delta\sigma_{isotope} = -0.664$ ppm.

The environment effect has two contributions:
(a) direct shielding

$$\Delta\sigma_0^{env} = -\int \frac{\Delta v(\vec{r})}{r^2}(1 - 3\cos^2\theta)d\vec{r} \quad ,$$

which cancels for a spherically symmetric environment (it is without directional solvation effects or H-bonds), and
(b) changes in the molecular properties, given above, which contribute to an extra chemical shift

$$\Delta\sigma_{gas-liquid} \sim (\bar{R}_{liq} - \bar{R}_{gas} + R_{e,liq} - R_{e,gas})\sigma' \quad ,$$

then $\Delta\sigma_{environment} \sim 1.95$ ppm, which should be the main contribution to the solvent effect.

Results for molecular H_2O in free space and in a liquid Br_2-like environment are shown in table 2.

Table 2
The water molecule

	H_2O exp.	H_2O free calc.	H_2O in Br_2 calc.	In liquid Br_2 (corrected)
Equilibrium distance Re (a.u.)	1.8090	1.7750	1.8350	
Equilibrium angle	104.46°	102.25°	101.00°	
E_{min} non-relativistic (without correlation) (Ry)	- 152.1350	- 152.5237	- 152.5719	
Correlation energy (Ry)	- 0.7402	- 0.4455		
ΔE binding (Ry)	- 0.6990	- 0.700		
f_{RHO} (Ry/(a.u.)^2)	0.5420	0.509	0.500	
q_{RHO} (Ry/(a.u.)^3)	0.6776	0.25	0.10	
f_{PHO} (Ry/(grad)^2)	0.002789	0.00580	0.0013	
R_{HH} (a.u.)	0.0422	0.0408		
$(\overline{R - R_e})_{HO}$ (a.u.)	0.03057	0.01235	0.00509	0.01250
$(\overline{R - R_e})_{HHO}$ (a.u.)	0.08870	0.03602	0.01480	0.03644
$(R - R_e)_{HO} - (R - R_e)_{HO}$ (a.u.)	0.05813	0.02363	0.00971	0.02394
$\sigma'_{OH} = 2\sigma/\delta R_{OH}$ (ppm/Bohr)		- 18.2		- 19.6
$\sigma'_{HH} = 3\sigma/\delta R_{HH}$ (ppm/Bohr)		- 2.038		

Using Ramsey's formalism, the chemical shifts computed for water are shown in table 3.

The computed ionization potentials for the water molecule are presented in table 4, together with the UV first absorption maximum calculated for the first allowed transition in water (A → X). For this transition energy, the $SW\chi_\alpha$ [12] calculation, using the transition state concept, gives a value of 0.7387 Ry, while the LCAO [12] method gives 1.6349 Ry (Koopman's theorem), to be compared to an experimental value of 0.552 Ry [16]. The LCAO result is expected because the Hartree-Fock virtual orbitals are poor approximations to excited

Table 3
Association and solvent chemical shifts for positive muons in water molecules in free space and in liquid Br_2-like environment (ppm)

		Exp.	Calculation	Scaled calculation[a]
$\Delta\sigma_{\text{isotope, gas phase}}$			- 0.2966	- 1.24
$\Delta\sigma_{\text{isotope, liquid}}$			- 0.18	- 0.471
$\Delta\sigma_{\text{liquid association}}$	(H_2O)	- 1.18[b]	- 0.96	
	$(MuHO)$		- 0.70	
$\Delta\sigma_{\text{total, association + isotope, liquid}}$			- 0.66	- 1.23
$\Delta\sigma_{MuHO\ (gas\text{-}liquid\ Br_2)}$			- 0.84	- 0.46

[a] The scaled calculation consists in a semiempirical scaling of f and g in the gas and in the liquid in such a way that the gas phase vibration parameters are reproduced. See last column of table 2.
[b] Taken from M. Camani et al., Hyp. Int. 6 (1979) 435.

Table 4
Calculated and experimental ionization potentials (Rydberg units) for water in the $^1A_1$: $(1a_1)^2$ $(2a_1)^2$ $(1b_2)^2$ $(3a_1)^2$ $(1b_1)^2$ state

State	I.P.-MSX_α[11]	I.P.-LCAO[12]	ab-initio-CHS (Slater orbs.)	ECBA[13]	ab-initio[14]
$1a_1$	- 40.1110	- 40.6342	- 38.757	- 39.6832	- 41.1219
$2a_1$	- 2.2113	- 2.5406	- 2.1799	- 2.3667	- 2.6997
$1b_2$	- 1.1551	- 1.2669	- 1.2305	- 1.3524	- 1.4321
$3a_1$	- 1.1359	- 1.0495	- 1.0335	- 1.0804	- 1.1669
$1b_1$	- 1.1010	- 0.9734	- 0.9525	- 0.9261	- 1.0141
First transition energy (in Rydberg units)					
This work	MSX_α	LCAO	SAp_1[10]		
0.570	0.7387	1.6349	0.552		

states orbitals. The MSX_α result gives too large a transition energy because the $1b_1$ orbital is too low. This is consistent with the overestimations of the $1b_1$ ionization potential.

4. Discussion

The electron gas exchange-correlation multiple scattering technique allows the introduction of an outer potential to represent environment effects on molecules in condensed phases. It is also useful to obtain parameters like the bond lengths and bond angles, the rate of change of chemical shielding constants with bond length and bond angles, binding energies and electronic spectra.

These results allow the quantitative analysis of the observed μ^+SR chemical isotope and solvent shifts.

A preliminary report of this paper, including only the first analysis of the HBr molecule, was presented at the First International Topical Meeting on Muon Spin Rotation held at Kurchoch, Switzerland, September 4-7, 1978 [15].

We are grateful for the financial support of the Consejo Nacional de Ciencia y Tecnología, México, Project IT.79/0196.

Appendix A

Total energy calculation within the self-consistent cellular multiple scattering method

Within the local density approximation for the electron-electron interaction two functionals of the electronic density $\rho(\vec{r})$ are needed: the effective local one-electron potential $V^{\sigma}(\vec{r})$ for spin σ electrons and the local exchange-electron energy density $\varepsilon_x(\vec{r}) = U^{\sigma}_{xc}(\vec{r})$.

The total energy, for the cellular multiple scattering technique, is written as the sum

$$\langle E_T \rangle = \langle E_I \rangle + \langle E_{nn} \rangle + \langle E_{ee} \rangle + \langle E_{xc} \rangle + E_{Ewald} \tag{A.1}$$

of the kinetic energy E_T, electron nuclear interaction energy E_{en} the electron-electron interaction energy E_{ee}, and the internuclear repulsion energy E_{nn} contributions. For the calculation of electric and magnetic properties, an extra term for the interaction of the system with the environment E_{Ewald} is added.

However, in practice the Kohn-Sham eigenvalues are used to compute the total energy, knowing the occupation n_i of states ϵ_i, from the expression

$$\langle E_T \rangle = \sum_i n_i \epsilon_i - \int V_c(\vec{r}) \rho(\vec{r}) d\vec{r} + \sum_{\sigma} \int \left(U^{\sigma}_{xc}(\vec{r}) - V^{\sigma}_{xc}(\vec{r}) \right) \rho_{\sigma}(\vec{r}) d\vec{r}$$

$$+ \frac{1}{2} \sum_{\alpha \neq \beta} \sum_{L} \frac{2 Z_{\alpha} Z_{\beta}}{R_{\alpha\beta}} \tag{A.2}$$

Here $V_c(\vec{r}) = V^{\sigma}(\vec{r}) - V^{\sigma}_{xc}(\vec{r}) - V^{\sigma}_{ext}(\vec{r})$ is called the "Coulomb electron-electron repulsion term" and will be computed from

$$V_c(\vec{r}) = \int \frac{\rho_T(\vec{r}') d\vec{r}'}{|\vec{r} - \vec{r}'|} \tag{A.3}$$

once the proper partitioning of the electron density $\rho(\vec{r})$ is found, as described in Appendix B.

The electron nuclear potential is as usual given by

$$V_{en}(\vec{r}) = -\sum_a \frac{2Z_a}{|\vec{r} - \vec{R}_a|} \quad , \tag{A.4}$$

considering all the nuclei of the cluster with charge Z_a held at the positions R_a and, finally, the exchange correlation term for electrons of spin s is obtained from

$$V_{xc}^s = V_x^s + V_c^s \ ,$$

$$V_{xc}^s(\vec{r}) = -a(n_s)G(\rho_s, n_s)\rho_s^{1/3}(\vec{r}) - \rho_{s'}(\vec{r})\rho_s^{-2/3}(\vec{r})C(\rho_s, \rho_{s'}, n_s) \ , \tag{A.5}$$

where $a(n_s)$, $G(\rho_s, n_s)$ and $C(\rho_s, \rho_{s'}, n_s)$ are given and derived in [5].

The total electronic density is taken to be a sum for spin s and the opposite spin s'

$$\rho(\vec{r}) = \rho_s(\vec{r}) + \rho_{s'}(\vec{r}) \ , \tag{A.6}$$

and, finally, the exchange correlation energy density

$$U_{xc}^s(r) = -F(n_s)\rho_s^{1/3}(1) - \frac{S(n_s)|\nabla\rho_s(1)|^2}{\rho_s^{7/3}(1)} - 0.1538\ (1 + 3.7723/n_s)^{-2/3}\rho_{s'}(1)\rho_s^{-2/3} \ , \tag{A.7}$$

$F(n_s)$ and $S(n_s)$ to be found, again, in ref.[5].

Eq.(A.2) states simply that the sum of the eigenvalues, weighted with the occupation numbers n_i, such that

$$\rho_{real}(\vec{r}) = \sum_i n_i \psi_i^*(\vec{r})\psi_i(\vec{r}) \ ,$$

is not the total electronic energy because first, the Coulomb interaction is taken twice because the same electron is considered as the origin of the potential $V_c(\vec{r})$ and, within the Kohn-Sham scheme, subject to the one-electron potential used to obtain the eigenvalues

$$\left(-\nabla^2 + V(\vec{r})\right)\psi_i(\vec{r}) = \varepsilon_i\psi_i(\vec{r}) \quad , \tag{A.8}$$

and, second, because the integral of the exchange correlation potential

$$\int V_{xc}^s(\vec{r})\rho_s(\vec{r})d\vec{r}$$

is not the exchange correlation energy, which should be obtained from the exchange correlation energy density $U_{xc}^s(\vec{r})$.

The cellular method assumes that the charge can be considered as a sum over N + 2 non-overlapping regions

$$\rho_s(\vec{r}) = \sum_{\substack{\text{region} \\ i=0}}^{N+1} \tilde{\rho}_s^i(\vec{r}_i) \qquad \vec{r}_i = \vec{r} - \vec{R}_i \ , \tag{A.9}$$

that is, in each region there is only one contribution $\tilde{\rho}_s^i(\vec{r}_i)$ within

the cell with reference origin $\vec{R}_i$. The cell's volume v_i can be defined

$$v_i = \int \Omega_i(\vec{r}) d\vec{r} \ , \tag{A.10}$$

then Ω_i is a step function with value 1 inside the cell (or region) and 0 outside of it.

The combination of formulae (A.9) and (A.10) implies that from the solutions (A.8) a cellular charge density has to be constructed (projected out). Besides, solutions to (A.8) are to be found for a cellular potential decomposed as a sum over N + 2 non-overlapping regions

$$V^{\sigma}(\vec{r}) = \sum_{i=0}^{N+1} \tilde{V}_i^{\sigma}(\vec{r}_i) \ , \tag{A.11}$$

to be constructed from the auxiliary wave functions $\tilde{\chi}_i(\vec{r})$ or better still from the projected densities $\tilde{\sigma}_i(\vec{r}_i)$ of (A.9). The energy densities could be found from the real density $\rho_{N+1}(\vec{r})$ or, the usual computational practice, from the cellular densities $\tilde{\rho}_i(\vec{r}_i)$ or their approximations.

Eqs. (A.9 – A.11) can be combined

$$\tilde{\rho}_i(\vec{r}_i) \cong \rho_i^{\sigma}(r_i)\Omega_i(\vec{r}_i) \ , \tag{A.12a}$$

$$\tilde{V}_i^{\sigma}(\vec{r}_i) \cong \tilde{V}_i^{\sigma}(r_i)\Omega_i(\vec{r}_i) \cong V_i^{\sigma}(r_i) \ , \tag{A.12b}$$

to obtain approximate potentials and charge densities which are angularly independent within each cell to simplify the evaluation of eqs. (A.2 – A.5) and (A.7). Within the cellular approximation $\rho_i^{\sigma,+} = \rho_i^{int} = \text{constant}$.

The cells could have, in principle, any shape; but because of approximations (A.12a) and (A.12b) and, moreover, because for the scattering matrices we assume

$$R_{LL'}^{i} = R_{ll'}^{i}\delta_{LL'} \qquad \text{for } l = 0,\ldots,l_{max} \ , \tag{A.13}$$

(that is, we find the scattering matrices from the angular independent part of (A.12b)), there is a practical need for using the lowest possible l_{max} in (A.13). The actual cells are taken to be truncated spheres centered around the atomic nuclei. In practice, the spheres enclosing the cells are not allowed to overlap more than 40–50% (Keller, 1973 [4]).

The cell's truncation is made on a plane surface including the common circle where two neighbouring cells begin to overlap before the truncation. The outer cell extends outside of a truncated sphere centered on the molecule or cluster. The truncation is made by allowing the atomic cell to prevail.

For the actual calculation, averages over the truncations are used and not the step functions themselves. This requires the use of the functions

$$\bar{\Omega}_i(r_i) = \frac{1}{4\pi} \int \Omega_i(\vec{r}_i) d\vec{r}_i$$

explicitly

$$\Omega_i(r_i) = \begin{cases} 0 & r_i > b_i \text{ (radius of the smallest sphere enclosing cell } i) \\ 1 - \sum_{\substack{j \neq i \\ j \neq 0}} h_{ij} \left(1 - a_{ij}/r_{ij}\right) * 1 - \sum_{\substack{j \neq i \\ j \neq 0}} h_{ij} \Omega^0_{ij}(r_{ij}) \end{cases} . \tag{A.14}$$

Here, $h_{ij} = H(r_{ij} - a_{ij})$ is the Heaviside function

$$H(x) = \begin{cases} 0 & x < 0 \\ 1 & x > 0 \end{cases} \tag{A.15}$$

and a_{ij} is the distance between the center of sphere i to the common truncation with sphere j:

$$a_{ij} = \frac{b_i^2 + R_{ij}^2 - b_j^2}{2 R_{ij}} \tag{A.16}$$

For the outer sphere

$$\Omega_o(r_o) = \begin{cases} 0 & r_o < b_o \\ 1 - \sum_{i \neq o} \frac{b_i - (r_o - R_{oi})^2}{a_{oi} - b_{oi}} h_{io} \end{cases} , \tag{A.17}$$

where $h_{io} = H(R_{oi} + b_i - r_o)$.

The degree of "cellularity" for each pair of atomic cells truncating each other can be defined as

$$\text{cellularity } \% = \frac{b_i + b_j - R_{ij}}{R_{ij}} \times 100 \tag{A.18a}$$

and for an atomic cell with an outer cell being truncated by it

$$\text{cellularity } \% = \frac{b_i + R_{oi} - b_o}{b_i} \times 100 . \tag{A.18b}$$

Appendix B

The cellular electronic density and potentials

Once the set of eqs. (17) has been solved within one iteration and the set of coefficients C_{lm} has been obtained, the wave function for cell i is given by

$$\psi^i(\vec{r}_i) = \sum_{l,m} \overline{r}^i_{lm}(r_i) Y_{lm}(\hat{r}_i) , \tag{B.1}$$

where $\vec{r}_i = \vec{r} - \vec{R}_i$. The integral of the charge density will be

$$\int_{\text{cell}} r^2 \sum_{\substack{L \\ L'}} \overline{r}^{i*}_{l',m'}(r) \overline{r}^i_{lm}(r) Y^*_{l',m'}(\hat{r}) Y_{lm}(\hat{r}) d\vec{r} , \tag{B.2}$$

and is not evaluated in practice. Instead it is approximated by an integral on the surface of the sphere to avoid mixing of the different angular momenta terms, as

$$\int_{\text{cell}} |\psi(\mathbf{r})|^2 d\tau \approx \int_{\text{cell}} |\psi(\mathbf{r})|^2 d\tau = \sum_{l,m} 4\pi |\bar{\psi}^l_{lm}(r)|^2 + 4\pi \sum_{l,m} |C^l_{lm}|^2 |\bar{\psi}^l_L(\xi)|^2 \,, \tag{B.3}$$

to obtain the renormalized coefficients C^l_{lm} such that the amount of charge per cell remains unchanged. The computer codes have a normalization subroutine to evaluate the $\bar{\psi}^l_{lm}(r)$ directly. This procedure introduces inaccuracies which are larger in the direction of the truncations and depend on the nature of the wave function lying within the truncated part of the cell.

The cellular density is finally given by

$$\rho^i_c(r) = \sum_{l,m} \frac{|C^l_{lm}|^2 |\bar{\psi}^l_L(r)|^2}{\Omega^i(r)} \,, \tag{B.4}$$

for each state.

B.1. The cellular electronic effective potential

There are two approximations used in practice:

(a) the electronic effective potential is to be obtained from the charge densities (B.4), and

(b) to keep for the construction of the angular independent potential of each cell terms where the corrections due to the truncations are up to first order in the functions (A.14) and (A.17) telling the part of the cell which is actually considered.

The cellular potential (Rydberg units) is:

(a) Outer region:

$$V^{\text{out}}(r) = \Omega_c(r) \left\{ \frac{2Q_{\text{cell}}}{r} + \frac{2}{r}\int_{b_0}^{r} 4\pi r'^2 \bar{\rho}^0_s(r')dr' + 2\int_{r}^{\infty} 4\pi r' \bar{\rho}^0_s(r')dr' \right.$$

$$\left. + V_{xc}\left[\rho^0_s(r)\right] + \sum_{i \neq 1}^{N} \frac{2(Q_i - Z_i)}{r} \right\} + (1 - \Omega_c(r))V^{\text{int}}$$

$$+ \Omega_c(r) \sum_{i \neq 1} \int_{r_{c_i}-b_{c_i}}^{r_{c_i}+b_{c_i}} 4\pi q_{i,0}(r') \left[\frac{1}{r'} - \frac{1}{r}\right] f_{c_i}(r')dr' \,, \tag{B.5}$$

defining $\bar{\rho}^0_s = \rho^0_s - \bar{\rho}^0_c$ and Z_i as the total electronic charge of cell i with nuclear charge $+Q_i$.

The first term on the right is the straightforward potential for the outer cell; the second is the correction arising from the fact that where the truncations are, the interstitial potential should be taken as a reference; the third represents corrections to be done because if the charges $q_{i,0}(r')$ of cell i are not inside the sphere with radius r within the outer cell but outside, then the potential should be proportional to $1/r'$ and not to $1/r$. These last corrections are, in fact, second order in the factors (A.14). The function of $f_{c_i}(r')$ will be different from unity if higher order corrections on the factors (A.14) are to be included. For the total energy calculation, the

terms between braces in (B.5) should be used when needed.

(b) Atomic cells. The one-electron potential to be used for the calculation of the phase shift is

$$V^{i*0}(r) = \Omega_i(r)\left\{-\frac{2Z_i}{r} - \sum_{j\neq i,o}\frac{2(Z_j-Q_j)}{R_{ij}} + \frac{2}{r}\int_0^r 4\pi r'^2\bar{\rho}_i^i(r')dr' + 2\int_r^{b_i} 4\pi r'\bar{\rho}_i^i(r')dr' + 2\overline{\frac{1}{R_i}}_{int}\overline{\rho}_{int}v_{int} + v_{xc}\left[\rho_i^i(r)\right]\right\} + (1-\Omega_i(r))v^{int} + \Omega_i(r)\sum_{j\neq i,o}B_{ij}\int_r^{b_j}\rho_{ij,i}(r')\left[\frac{1}{r'}-\frac{1}{R_{ij}}\right]f_{ji}(r')dr' \tag{B.6}$$

with

$$\overline{\frac{1}{R_i}}_{int}v_{int} = 2\pi\left(\max(R_{oj}+b_j,b_o)\right)^2 + \frac{1}{3}\pi R_{oi}^2 - \overline{\frac{1}{r_i}}v_i - \sum_{j\neq i,o}\frac{v_j}{R_{ij}} - \int_{b_o}^{\max(r_{oj}+b_j,b_o)} 4\pi\bar{\rho}_o(r_o)r\,dr_o \tag{B.7}$$

and $\max(R_{oj}+b_j,b_o)$ is the largest of $R_{oj}+b_j$ (or b_o) for the cluster and the average

$$v_i\overline{r_i^n} = \int_o^{b_i} 4\pi\Omega_i(r_i)r_i^{n+2}dr_i \tag{B.8}$$

has been used.

(c) Interstitial region. The potential (in Rydbergs) is

$$V^{int} = \frac{1}{v_{int}}\left\{\sum_{i=1}^{N}\overline{\frac{2}{R_i}}_{int}(Z_i-Q_i+\bar{\rho}_{int}v_{int}) + 2\bar{\rho}_{int}\left\{\frac{8}{3}\pi^2\left[\frac{(\max(R_{oj}+b_j,b_o))^3}{3} - \sum_{i=1}^{N}\left(\frac{R_{oi}^2v_i}{4\pi}+\overline{r_i^2}v_i\right) - \int_{b_o}^{\max(R_{oj}+b_j,b_o)} r_o^2\bar{\rho}_o(r_o)dr_o\right] + 2\pi\left(\max(R_{oj}+b_j,b_o)\right)^2 + V_{xc}\left[\rho_{int}\right]\right\} + 2\int_{b_o}^{\infty} 4\pi r_o'^2\bar{\rho}_s^o(r_o')r_o'dr_o' + \frac{2\bar{\rho}}{v_{int}}\overline{<\Delta r^2>}_{int}\right\}. \tag{B.9}$$

The last term on the right contains second and higher order corrections. The interstitial charge $\bar{\rho}_{int}$ is assumed to be uniform.

The deduction of (B.6), (B.7) and (B.9) is straightforward if

the spherical average of the inverse distance between i and j

$$\overline{\frac{1}{|\vec{r}_i - \vec{r}_j|}} = \frac{1}{r_>} \quad ; \quad r_> = \max(|\vec{r}_i|, |\vec{r}_j|) \ ,$$

is considered.

References

[1] M. Camani, F.N. Gygax, E. Klempt, W. Rüegg, A. Schenck, H. Schilling, F. Schulze and H. Wolf, Hyp. Int. 6(1979)425.
[2] J. Keller, paper presented at the Fermion Symposia (1977), published in Int. J. Quant. Chem. 9 (1975)563.
[3] J.L. Gázquez and J. Keller, Phys. Rev. A16(1977)1358.
J.L. Gázquez, M. Ortiz and J. Keller, Int. J. Quant. Chem. Symp. 13 (1979)277.
S. Keller and J.A. Gázquez, Phys. Rev. A23(1979)1169.
[3a] W. Kohn and L.J. Sham, Phys. Rev. 140(1965)A1133.
[4] J. Keller, J. de Phys. Colleq. C3(1972)241.
J. Keller, Adv. Quant. Prot. Ch. 10, part 1 (1972)514.
J. Keller, in: Computational methods for large molecules and localized states in solids, ed. F. Herman, A.D. McLean and R.K. Nesbet, Proc. Symp. 1972 (Plenum, New York, 1973), p.111.
J. Keller, in Computers in chemical education and research, ed. E.V. Ludeña, E.B. Sabelli, and A.C. Wahl (Plenum, New York, 1977) p.225.
[7] The use of cylindar symetry is further discussed in: A. Garrit, J.L. Gázquez, M. Castro and J. Keller, Int. J. Quant. Chem. 15 (1979)731.
F. Blas, thesis, Fac. de Química, U.N.A.M., Méx. 1976, for the particular case of the water molecule.
[8] D. Bressanini and A. Nanofalvy, Phys. Lett. 33B(1970)309.
[9] R.W. Williams, Phys. Lett. 34B(1971)163.
[10] N.F. Ramsey, Phys. Rev. 78(1950)699.
[11] R. Pixman, J. Chem. Phys. 36(1962)679.
[12] J.W.D. Connolly and K.H. Sabin, J. Chem. Phys. 56(1972)5529.
[13] K. Siegbahn, C. Nordling, G. Johansson, J. Hedman, P.F. Hedén, K. Hamrin, U. Gelius, T. Bergmark, L.O. Werme, R. Manne and Y. Baer, ESCA applied to free molecules (North-Holland, Amsterdam, 1969)
A.W. Potts and W.C. Price, Proc. Roy. Soc. A326(1972)181.
[14] B.J. Rosenberg and I. Shavitt, J. Chem. Phys. 63(1975)2162.
[15] M. Castro, J. Keller and A. Schenck, Hyp. Int. 8(1979)439.
[16] G. Herzberg, Molecular spectra and molecular structure, (III). Electronic spectra and electronic structure of polyatomic molecules, (Van Nostrand, Princeton, N.J., 1966).

Ground state of the He_2^{2+} molecular ion computed with density functional techniques

Miguel Castro and Jaime Keller

Departamento de Química Teórica, Facultad de Química, U.N.A.M., Mexico 20, D.F.

Oscar N. Ventura

Cátedra de Química Cuántica, Facultad de Química, Avda. Gral. Flores 2124, Montevideo, Uruguay

(Received 10 June 1982; accepted 24 August 1982)

Total energy calculations in statistical exchange multiple scattering techniques[1] allow the analysis of a large variety of problems. Molecular orbital eigenvalues have been used with relatively good success to study spectra and related properties of molecules. The improvement of the results by means of cellular techniques[2] results in energy analysis of Hartree–Fock quality, allowing the estimation of bond lengths, bond angles, vibrational constants, and especially of magnetic states and of the effect of self-exchange and exchange in determining the ground state. Calculations where the accuracy to be expected can be calibrated are very important and this is the purpose of the present note.

Molecules with only a few electrons are a severe test to density functional techniques. In a previous article (hereafter referred as I) we have discussed the effect of space partitioning in multiple scattering techniques as applied to the H_2^+ molecular ion and the hydrogen molecule.[3]

In this letter we want to comment further on the cellular space partitioning and statistical exchange, choosing the He_2^{2+} molecular ion as the subject of our study. Cellular partitioning is obtained by allowing the atomic (muffin tin) spheres to grow avoiding overlap by truncating the cells with planes passing through the contact circles and allowing the atomic cells to truncate the center sphere.

Although He_2^{2+} has never been observed in its ground state, there have been some calculations on it[4,5] and on its excited states[6,7] particularly in relation to the reaction of alpha particles with helium atoms. In this connection we find that some of the correlation energy may be obtained employing the nonpaired spin-molecular-orbitals formulation required to obtain the correct atomic dissociation limit, as compared with more sophisticated calculations.

Our calculations were done as described in I in its Hartree–Fock and Hartree versions (i.e., with and without including exchange) using the cellular multiple scattering, X_{α} method. The determination of the sizes of the different regions was done by minimization of the interstitial charge as previously reported,[1–3] and the spin segregation or nonpaired spin-molecular-orbitals method was included in the cellular X_{α} calculations.

The optimum space partitioning, that of minimum interstitial charge within the approximations of the method and the computer codes, is obtained for $R_{He}/d_{He-He} = 0.6466$, where R_{He} is the radius of the smallest sphere enclosing the He cell. The "cellularity" for this

 0021-9606/82/246348-03$02.10

TABLE I. Total energy values (in Ry) for different internuclear distances d (in bohrs). The symbols have the following meaning: $X_{\alpha\beta}$, cellular method, $\alpha\beta$-statistical exchange, spin segregated; CH, cellular method Hartree (without self-exchange or self-Coulomb); SCHF single configuration LCAO MO SCF calculation (Ref. 5); SCHF+CI, the same but including CI (12 configurations) (Ref. 5); KR9, Kolos and Roothaan calculation using James and Coolidge nine-term polynomial (Ref. 4); KR40, the same but using the James and Coolidge 40-term polynomial (Ref. 4).

d	$X_{\alpha\beta}$	CH	SCHF	SCHF+CI	KR9	KR40
1.0					−7.099	−7.199
1.1	−7.252	−7.046	−7.215	−7.268		−7.297
1.2	−7.266	−7.066	−7.239	−7.313	−7.218	−7.343
1.3	−7.302	−7.092	−7.261	−7.331	−7.242	−7.359
1.4	−7.307	−7.089	−7.270	−7.339		−7.355
1.5	−7.302	−7.092	−7.181	−7.318		
1.6	−7.299	−7.042	−7.097	−7.301	−7.135	−7.319
1.7	−7.274	−7.014	−7.042	−7.283		
1.8	−7.256	−6.982	−6.998		−7.048	−7.271
2.0	−7.222	−6.907	−6.913	−7.246	−6.960	
2.1	−7.210	−6.876	−6.891	−7.242		

radius is 39.39% over the muffin tin spheres.

Once the optimum cell's size was calculated we proceed to consider the potential energy curves. The results obtained including or neglecting the self-exchange as well as the values given by other methods[4,5] are given in Table I and the potential energy curves have been drawn in Fig. 1.

From the comparison of the cellular Hartree calculation with the Kolos–Roothaan curves and the SCF ones we can see the error introduced in the minimum energy by the partitioning of the space. Both, because of the shapes of the curves for large internuclear distances and because of the neglecting of correlation in the cellular Hartree calculation, this curve must be compared with the Kolos–Roothaan nine-term polynomial and the Fraga–Ransil SCHF calculations. This comparison shows that space partitioning (in the cellular method) produces an underestimation of the electronic energy of approximately 1.5 eV (or 0.56% of the total electronic energy of this two-electron molecular ion).

When the $\alpha\beta$-statistical exchange is taken into account the overstimation of the self-exchange compensates the positive energy error of the space partitioning. As long as the spin segregation method gives very similar values to the standard molecular orbitals for internuclear distances shorter than 2.0 bohr (see I) the result can be described entirely to the goodness of the $\alpha\beta$-statistical exchange. Indeed, the error in the total energy (obtained by comparison with the accurate Kolos–Roothaan 40-term polynomial value) is only 0.8 eV. It is of the same order of magnitude as the correlation energy obtained as the difference between the KR40 and SCFCI minima (approximately 0.3 eV). This amounts to a cancellation of the space partitioning and statistical exchange inaccuracies and means that a separate discussion of any one of the two will lead to a larger estimated error.

A final important point to be noted is that the spin

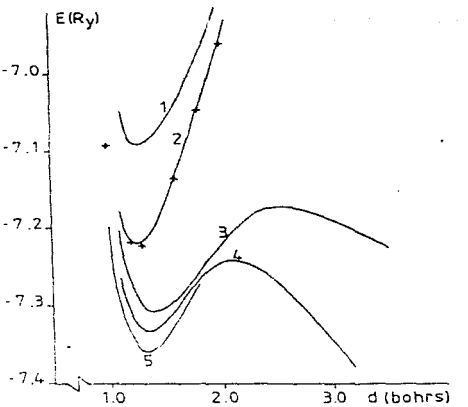

FIG. 1. Total energy (in Ry) vs internuclear distance d (in bohrs) curves for the He_2^+ molecular ion. (1) Cellular calculation Hartree (without self-exchange or self-Coulomb). (2) Single configuration Hartree–Fock calculation (Ref. 5). The superimposed crosses are the values calculated according to the nine-term polynomial of Kolos and Roothaan (Ref. 4). (3) $X_{\alpha\beta}$ spin segregated calculation (this work). (4) Single configuration Hartree–Fock plus CI calculation (only 12 configuration included in CI) (Ref. 5). (5) 40-term Kolos and Roothaan polynomial calculation of (Ref. 4).

segregated $X_{\alpha\beta}$ calculation reproduces (in part, at least) the trend of the SCFCI curve for large internuclear distances. This has been reported before for the H_2 molecule in I but it is specially important here because the CI results clearly indicate He_2^+ to be a metastable molecule a fact also suggested by the cellular $X_{\alpha\beta}$ and the free atom calculations. Indeed, this is a good example to show that the density functional methods can predict both the stability of a molecule as the RHF method and the correct atomic dissociation limit as UHF despite a generalized criticism of the local density approximation made recently.[6]

We acknowledge the help of Dr. Manuel Braga in the first steps of this work.

[1]For the computational method and total energy calculations as used in the paper, see M. Castro, J. Keller, and P. Ilius, Hyperfine Interactions (to be published). The basic earlier references to multiple scattering techniques are: L. Eyges, Phys. Rev. 111, 683 (1958); B. Segall, Am. Phys. Soc. Bull. 1, 5405 (1959); J. C. Slater, J. Chem. Phys. 43, S228 (1965); K. H. Johnson, J. Chem. Phys. 45, 3085 (1966); K. H. Johnson, Int. J. Quantum Chem. 1S, 361 (1967); F. C. Smoth and K. H. Johnson, Phys. Rev. Lett. 22, 1168 (1969); K. H. Johnson, in *Advances in Quantum Chemistry*, edited by P. O. Lowdin (Academic, New York, 1971), p. 143; J. Korriga, Physica 13, 392 (1947); W. Kohn and N. Rostoker, Phys. Rev.

94, 1111 (1954); J. M. Ziman, Proc. Phys. Soc. 86, 337 (1965); P. W. Anderson and W. L. McMillan, in *Proceedings International School of Physics Enrico Fermi*, edited by W. Marshall (Academic, New York, 1967); L. Schwartz and H. Ehrenreich, Ann. Phys. 64, 100 (1971); R. Evans and J. Keller, J. Phys. C 4, 3155 (1971).
[2]J. Keller, Int. J. Quantum Chem. Quantum Chem. Symp. 9, 583 (1975); J. Keller, J. Phys. (Paris), Colloq. C 3, 241 (1972); J. Keller, AIP Conf. Proc. 10, Pt. 1, 514 (1972); J. Keller, in *Computational Methods for Large Molecules and Localized States in Solids*, edited by F. Herman, A. D. McLean, and R. K. Nesbet (Plenum, New York, 1973), p. 341; J. Keller, in *Computers in Chemical Education and Research*, edited by E. V. Ludeña, N. H. Sabelli, and A. C. Wahl (Plenum, New York, 1977), pp. 225–260.
[3]A. Garritz, J. L. Gázquez, M. Castro, and J. Keller, Int. J. Quantum Chem. 15, 731 (1979).
[4]W. Kolos and C. C. J. Roothaan, Rev. Mod. Phys. 32, 219 (1960).
[5]S. Fraga and B. J. Ransil, J. Chem. Phys. 37, 1112 (1962).
[6]J. C. Browne, J. Chem. Phys. 42, 1428 (1965).
[7]D. M. Bishop and L. M. Cheung, Mol. Phys. 38, 1475 (1979).
[8]M. M. Goodgame and W. A. Goddard III, Phys. Rev. Lett. 48, 135 (1982).

LINUS PAULING INSTITUTE of SCIENCE and MEDICINE
440 Page Mill Road, Palo Alto, California 94306
Telephone: (415) 327-4064

6 January 1983

Drs. M. Castro and J. Keller
Department of Theoretical Chemistry
Faculty of Chemistry
UNAN
Mexico 20, DF Mexico
and
O. N. Ventura
Department of Quantum Chemistry
Faculty of Chemistry
Avenida Gral. Flores 2124
Montevideo
Uruguay

Dear Drs. Castro, Keller and Ventura:

I was interested to read your paper in the Journal of Chemical Physics, 77, 6348 (1982).

I am writing to mention to you that I published a quantum mechanical treatment of the normal state of the doubly charged helium molecule ion just fifty years ago, in January 1933, in the Journal of Chemical Physics, Vol. 1, No. 1, page 56 (1933). The energy curve that I got was rather like your curve No. 4, single configuration Hartree-Fock plus CI calculation. My value for the internuclear distance is 1.49 a_0, for the dissociation energy 0.103 Ry, and for vibrational frequency 3200 cm^{-1}. I enclose copies of the paper.

Sincerely,

Linus Pauling

L.P:dm